© 2020. Published by The Company of Biologists Ltd | Journal of Cell Science (2020) 133, jcs245357. doi:10.1242/jcs.245357

RESEARCH ARTICLE

TMEM147 interacts with lamin B receptor, regulates its localization and levels, and affects cholesterol homeostasis

Andri Christodoulou[1,‡], Giannis Maimaris[1], Andri Makrigiorgi[1], Evelina Charidemou[1], Christian Lüchtenborg[2], Antonis Ververis[1,*], Renos Georgiou[1], Carsten W. Lederer[3], Christof Haffner[4], Britta Brügger[2] and Niovi Santama[1,‡]

ABSTRACT

The structurally and functionally complex endoplasmic reticulum (ER) hosts critical processes including lipid synthesis. Here, we focus on the functional characterization of transmembrane protein TMEM147, and report that it localizes at the ER and nuclear envelope in HeLa cells. Silencing of *TMEM147* drastically reduces the level of lamin B receptor (LBR) at the inner nuclear membrane and results in mistargeting of LBR to the ER. LBR possesses a modular structure and corresponding bifunctionality, acting in heterochromatin organization via its N-terminus and in cholesterol biosynthesis via its sterol-reductase C-terminal domain. We show that TMEM147 physically interacts with LBR, and that the C-terminus of LBR is essential for their functional interaction. We find that TMEM147 also physically interacts with the key sterol reductase DHCR7, which is involved in cholesterol biosynthesis. Similar to what was seen for LBR, *TMEM147* downregulation results in a sharp decline of DHCR protein levels and co-ordinate transcriptional decreases of *LBR* and *DHCR7* expression. Consistent with this, lipidomic analysis upon *TMEM147* silencing identified changes in cellular cholesterol levels, cholesteryl ester levels and profile, and in cellular cholesterol uptake, raising the possibility that TMEM147 is an important new regulator of cholesterol homeostasis in cells.

This article has an associated First Person interview with the first author of the paper.

KEY WORDS: ER transmembrane proteins, LBR, Cholesterol, Sterol reductases

INTRODUCTION

The endoplasmic reticulum (ER) is the most extensive intracellular membranous compartment, consisting of a network of interconnected flat sheets and tubules, and the contiguous nuclear envelope (NE) (Baumann and Walz, 2001; Lynes and Simmen, 2011). The ER, as the site of protein synthesis, processing and assembly and membrane and lipid supplier of the cell, exhibits not only morphological but also functional compartmentalization (Baumann and Walz, 2001; Chen et al., 2013; Hu et al., 2011; Goyal and Blackstone, 2013; Lin et al., 2012; Shibata et al., 2006). Understanding how structural and functional specificity is formed and maintained is an ongoing challenge.

In our work on ER membrane morphogenesis (Santama et al., 2004; Christodoulou et al., 2016), we recently focused on transmembrane protein TMEM147, a 25 kDa protein that localizes to ER membranes (Dettmer et al., 2010; Rosemond et al., 2011) and possesses seven transmembrane domains with its N-terminus residing in the ER lumen and its C-terminus facing the cytosolic side of the membrane. The amino acid sequence of TMEM147 is highly conserved among mammalian species (human, rat, bovine and mouse sequences are 99% identical) and it is expressed at constant levels across many human tissues (Rosemond et al., 2011). TMEM147 was found to exhibit intricate reciprocal interactions with the ER proteins nicalin and NOMO (NOMO1,-2 and -3) and be a core component of a complex involving all three proteins that is important for early embryonic Nodal signaling in vertebrates (Dettmer et al., 2010). Furthermore, TMEM147 has been shown to influence forward trafficking, via the ER, of the muscarinic acetylcholine receptor M3R (CHRM3) (Rosemond et al., 2011). Both studies indicate important protein interactions of TMEM147 within the ER; its function, however, is still unknown.

At the onset of our experiments, we detected interactions between TMEM147 and lamin B receptor (LBR), which we fully characterize in this work (see Results). LBR is an extensively studied cellular protein that localizes to the inner nuclear membrane (INM). Its nucleoplasmic, hydrophilic N-terminus [amino acids (aa) 1–208 in human, including a chromatin-binding Tudor domain] was found to interact with lamin B (hence its name) and heterochromatin-associated proteins (HP1 and MeCP2) (Makatsori et al., 2004; Pyrpasopoulou et al., 1996; Worman et al., 1988). Through these interactions, LBR is assumed to provide a platform for internal nuclear organization by mediating the deposition of repressed and transcriptionally inactive heterochromatin to the NE periphery. The C-terminus of LBR (aa 208–615) is proposed to contain 8–10 transmembrane domains, whose topological organization within the INM is not settled in literature, and a short C-terminal 'tail' whose localization can be either nucleoplasmic or within the lumen between the outer and inner NE sheets (Olins et al., 2010).

A fascinating aspect of LBR structure is that, while the N-terminal part has a distinct nuclear function, unexpectedly, its C-terminus resembles C-14 sterol reductase enzymes (Li et al., 2015; Silve et al., 1998; Worman et al., 1990). In fact, the intron between exons 4 and 5 in the LBR gene is 10 kb long, raising the possibility that the gene may have evolved from a recombination event between two primordial genes, giving rise to a chimeric protein (Schuler et al., 1994; Olins et al., 2010). Specifically, LBR displays significant

[1]Department of Biological Sciences, University of Cyprus, 1678 Nicosia, Cyprus. [2]Biochemistry Center (BZH), University of Heidelberg, 69120 Heidelberg, Germany. [3]Department of Molecular Genetics Thalassaemia and Cyprus School of Molecular Medicine, The Cyprus Institute of Neurology and Genetics, 1683 Nicosia, Cyprus. [4]Institute of Stroke and Dementia Research, University of Munich, 81377 Munich, Germany.
*Present address: Neurogenetics Department and Cyprus School of Molecular Medicine, The Cyprus Institute of Neurology and Genetics, Cyprus.

‡Authors for correspondence (santama@ucy.ac.cy; christodoulou.c.andri@ucy.ac.cy)

A.C., 0000-0001-7151-6408; E.C., 0000-0002-2299-9471; A.V., 0000-0003-1798-6550; R.G., 0000-0002-2415-9230; C.W.L., 0000-0003-3920-9584; N.S., 0000-0002-8370-8674

Handling Editor: Arnoud Sonnenberg
Received 18 February 2020; Accepted 2 July 2020

Journal of Cell Science (2020) 133, jcs245357. doi:10.1242/jcs.245357

sequence similarity over its C-terminus with two key sterol reductases involved in late, post-squalene and smooth ER-localized steps of cholesterol biosynthesis; the C-terminus of LBR is 37% identical and 62% conserved with the 7-dehydrocholesterol reductase DHCR7, and 58% identical or 75% conserved with the 3 β-hydroxysterol Δ-14 reductase TM7SF2. Additionally, LBR harbors two 'sterol reductase family signatures 1 and 2' within its C-terminus, short motifs with similarities to many sterol reductases, including TM7SF2 and DHCR7 (Olins et al., 2010).

Functionally, human LBR complements the TM7SF2-like C14 sterol reductase ERG24 in *Saccharomyces cerevisiae* (Silve et al., 1998), and both LBR and TM7SF2 complement ERG3 reductase in *Neurospora crassa* (Prakash et al., 1999). Furthermore, it has been demonstrated that LBR is required for viability under cholesterol starvation conditions, and is constitutively expressed and essential for cholesterol synthesis, despite the presence of sterol-inducible TM7SF2 in human *LBR*-knockout cell lines (Tsai et al., 2016). The same study documented that the C-terminal sterol reductase domain of LBR alone is both necessary and sufficient for cholesterol production in HeLa cells and, importantly, nonsense LBR mutations, associated with Greenberg skeletal dysplasia or Pelger–Huët human congenital disorders of cholesterol metabolism, fail to rescue the cholesterol auxotrophy of an LBR-deficient human cell line (Tsai et al., 2016). Although LBR and TM7SF2 catalyze the same biosynthetic step and it appears that they provide some compensatory redundancy, their functional interactions are far from clear. Deletion of mouse *Tm7sf2* does not impair cholesterol biosynthesis (Bennati et al., 2008) and, interestingly, a small-molecule inhibitor of TM7SF2 drives oligodendrocyte differentiation from progenitor cells and induces oligodendrocyte remyelination via the concomitant accumulation of the intermediate 8,9-unsaturated sterol (Hubler et al., 2018).

Mutations in DHCR7, characterized by a cholesterol deficit and 7DHC precursor accumulation, are the cause of Lemli–Optiz syndrome (SLOS), the most common cholesterol metabolic disorder (Fitzky et al., 1998; Wassif et al., 1998; Waterham et al., 1998; Tint et al., 1994). Reduced cholesterol levels in SLOS impair hedgehog signaling by inhibiting the appropriate ciliary localization and activation of the smoothened receptor (Blassberg et al., 2016). The understanding of the molecular interactions between DHCR7 and LBR in cholesterol synthesis, pursued in mouse double knockout studies, remains incomplete (Wassif et al., 2007).

Thus, the overall functional interrelationships between LBR, TM7SF2 and DHCR7 in cholesterol biosynthesis require further elucidation. The role of LBR as a multitasking protein at the INM, the possible co-ordination between its dual role and its regulation also remain focal points of interest. In this work, we present new findings showing that the ER transmembrane protein TMEM147 drastically influences LBR levels and LBR targeting to the INM and impacts on cellular cholesterol levels by regulating both LBR and DHCR7.

RESULTS

TMEM147 localizes at the ER and NE in HeLa cells

Extending our interest in the role of ER-transmembrane proteins on ER morphogenesis and function (Christodoulou et al., 2016), we focused in this work on the characterization of TMEM147 (also known as NIFIE14; NM_032635.4) in human cells. Because of lack of an antibody suitable for immunofluorescence, we pursued transient transfections with an N-terminally FLAG-tagged full length *TMEM147* cDNA in HeLa cells; this revealed labeling of both the ER (Fig. 1A1,A2), consistent with previous findings (Dettmer et al., 2010; Rosemond et al., 2011), and also of the nuclear rim (Fig. 1A1; this is also visible with COS-7 cells in fig. 5A of Rosemond et al., 2011). We subsequently constructed a stable cell line, HeLa-TMEM147-GFP, constitutively expressing C-terminally GFP-tagged TMEM147. In these cells, TMEM147–GFP displayed the same distribution as the FLAG-tagged version (Fig. 1B1,B2) and confirmed colocalization at the ER upon double labeling with the ER marker protein calnexin (Fig. 1C1–C3) and overlap at the NE upon double labeling with the INM marker Lap2β (Fig. 1D1–D3).

Silencing of TMEM147 downregulates protein levels of LBR

To probe the function of TMEM147, we used RNAi as a tool. We established conditions for reliable siRNA-mediated silencing of *TMEM147*: typically, *TMEM147* mRNA levels were reduced down to 2.10±1.87% (mean±s.e.m.) or by a factor of 47.42 (P<0.0001) compared to what was detected with negative control silencing (mock silencing without siRNAs), as assessed with RT-qPCR (Fig. 2A). In silenced HeLa cells, TMEM147 protein levels, as assessed by quantitative western blot (WB) analysis, represented only 13.36±2.27% (mean±s.d.; P=0.0011) of negative control levels (Fig. 2B,C). When silencing was repeated in the stable HeLa-TMEM147-GFP cell line, it was accompanied by loss of GFP signal in immunofluorescence experiments (as a proxy for TMEM147–GFP expression) in silenced cells only, and not in negative control cells (Fig. 2D, compare D2 and D4), and by a marked reduction of signals for both native TMEM147 and TMEM147–GFP proteins as determined by WB analysis (Fig. 2E).

One consistent observation with *TMEM147* silencing was decreased cell viability compared with negative control cells, specifically affecting growth at late stages post-transfection (48–72 h) (Fig. 3A). In addition, the most striking result upon *TMEM147* silencing was our observation of a concomitant drastic reduction of levels of INM LBR, which could be detected at earlier time points (already by 48 h). As shown by representative WB experiments in Fig. 3B, LBR is consistently and significantly downregulated. Quantification showed LBR protein levels reaching only 9.93±6.23% (P=0.0065; mean±s.d.) of negative control levels (Fig. 3C), a reduction closely resembling that typically obtained for the TMEM147 protein itself (Fig. 2C). By comparison, the relative levels of emerin, another INM integral protein, and those of the protein-folding chaperone and ER integral protein calnexin, were not detectably altered (Fig. 3B).

The defining reduction of LBR protein was also visualized by confocal microscopy, revealing that specifically in *TMEM147*-silenced cells, LBR is hardly detectable at the INM (Fig. 3, compare panels D3 and D6), while lamin A, a nuclear lamina constituent demarcating the INM, is essentially unaffected (Fig. 3D2 and D5). The loss of immunofluorescence signal for LBR upon *TMEM147* silencing in HeLa cells (also seen by wide-field microscopy; Fig. S1A1–B3) was recapitulated in the stable HeLa-TMEM147-GFP cell line, in which loss of GFP signal (Fig. S1C1,D1) was accompanied by corresponding disappearance of LBR label in the same cells (see Fig. S1C2,D2, and C3 and D3 for overlays).

We sought to further examine the specificity of the observed effect of *TMEM147* silencing on LBR protein by utilizing an alternative siRNA (oligo#2), targeting a more downstream exon sequence than that used in the previous experiments (oligo#1) (#oligo1 and oligo#2 are shown in Fig. S2A, displaying part of the gene sequence and a TMEM147 protein membrane topology model). Silencing of *TMEM147* with oligo#2 not only effectively reduced TMEM147 protein levels but, again, also decreased LBR

Journal of Cell Science (2020) 133, jcs245357. doi:10.1242/jcs.245357

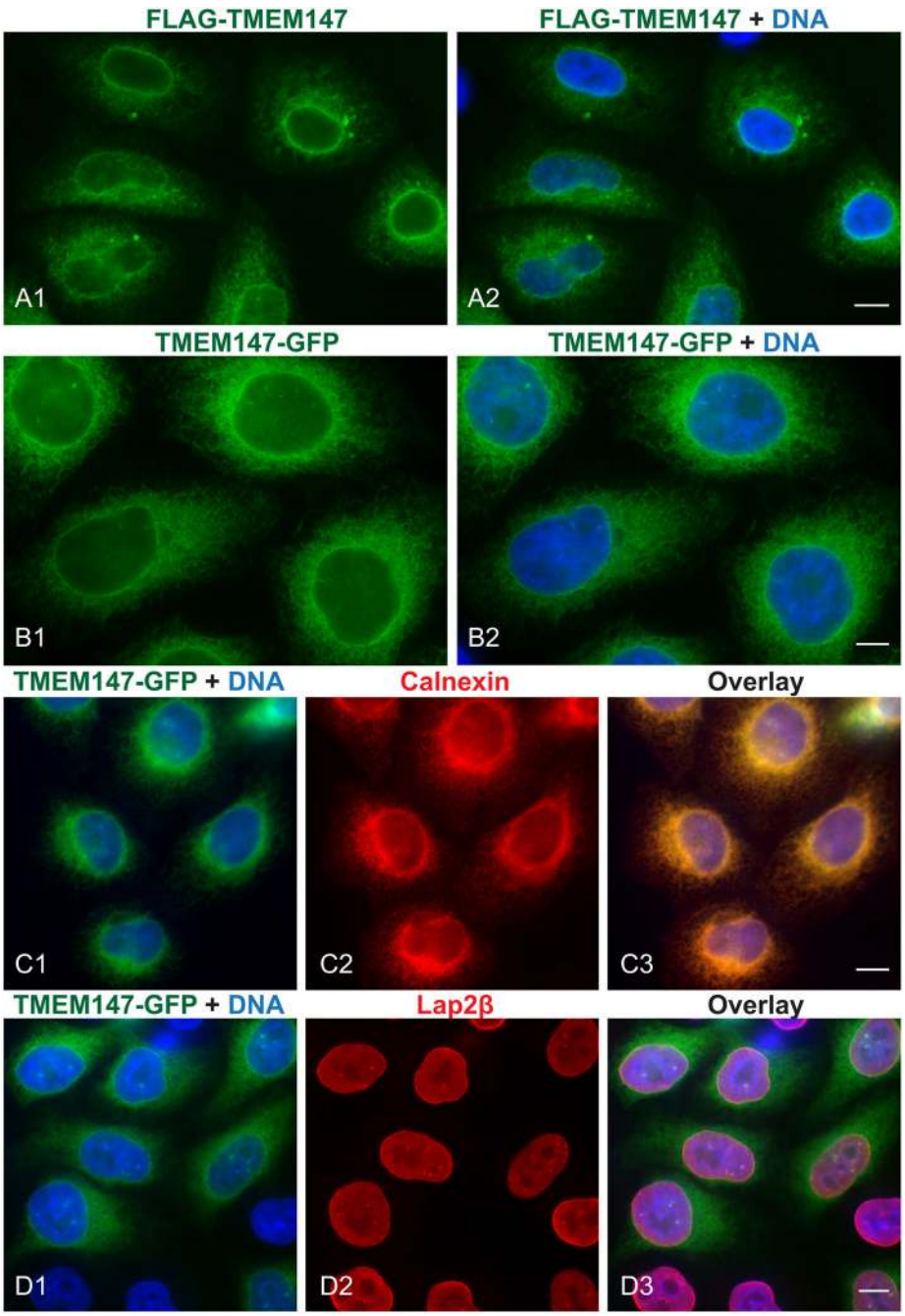

Fig. 1. Localization of TMEM147 at the ER and NE. (A1,A2) Immunofluorescence images of HeLa cells transiently transfected with plasmid expressing FLAG–TMEM147 reveal labeling of the ER and NE. FLAG immunoreactivity corresponds to green fluorescence (A1) and nuclear counterstain by Hoechst to blue fluorescence in overlay image (A2). (B1,B2) Immunofluorescence images of the TMEM147–GFP stable HeLa cell line, similarly, exhibit GFP fluorescence at the ER and nuclear rim (B1). Nuclei in blue in overlay image (B2). (C1–C3) Confirmation of ER labeling of TMEM147–GFP. Overlay of GFP (green) and nuclear staining (blue) is shown in C1. Concurrent immunolabeling for ER marker calnexin (red; C2) reveals a signal that overlaps with GFP signal in overlay image of all colors (C3). (D1–D3) Confirmation of NE labeling of TMEM147–GFP. GFP fluorescence (green; D1) and INM marker protein Lap2β immunofluorescence (red; D2) displays a yellow rim of overlap around the nucleus in overlay image D3. Scale bars: 10 µm (A,C,D); 5 µm (B).

levels, as observed by WB analysis (Fig. S2B), and visibly reduced LBR immunofluorescence signal, compared to negative control cells (Fig. S2, compare panels C2 and D2).

These data, therefore, show that reduction of TMEM147 results in a concomitant reduction of LBR protein at the INM.

Silencing of TMEM147 causes mislocalization of LBR to the ER

To analyze the cellular phenotype resulting from *TMEM147* silencing and its specific effect on LBR in more depth, we conducted a quantitative morphometric comparison in four independent experiments of *TMEM147*-silenced cells (n=48 cells) and negative control cells (n=55) labeled with anti-LBR antibody and Hoechst stain and optically sectioned by confocal microscopy (Fig. 4A1 and A2). Quantification of LBR mean fluorescence intensity in all cells was in line with our quantification of LBR protein levels by WB analysis, and again confirmed the significantly reduced signals in *TMEM147*-silenced vs control cells (P<0.0001) (Fig. 4B1). Interestingly, quantitation of Hoechst fluorescence in the same cells also revealed a clear reduction of Hoechst incorporation, indicative of loss of chromatin compaction specifically in *TMEM147*-silenced cells (P<0.0001) (Fig. 4A3,A4 and B2) and, consistent with this, a clear reduction of histone H3K9 methylation, serving as a heterochromatin marker and anchor of chromatin to the nuclear lamina (reviewed by Mattout et al., 2015) (Fig. 4A5,A6). Additionally, *TMEM147* silencing appeared to introduce changes in nuclear shape (altered sphericity, P<0.0001), presumably due to changes in the shape of the INM, where LBR resides (Fig. 4B3).

Using the stacks of optical sections for all 103 cells analyzed above, we produced 3D-rendered images which revealed a striking

Journal of Cell Science (2020) 133, jcs245357. doi:10.1242/jcs.245357

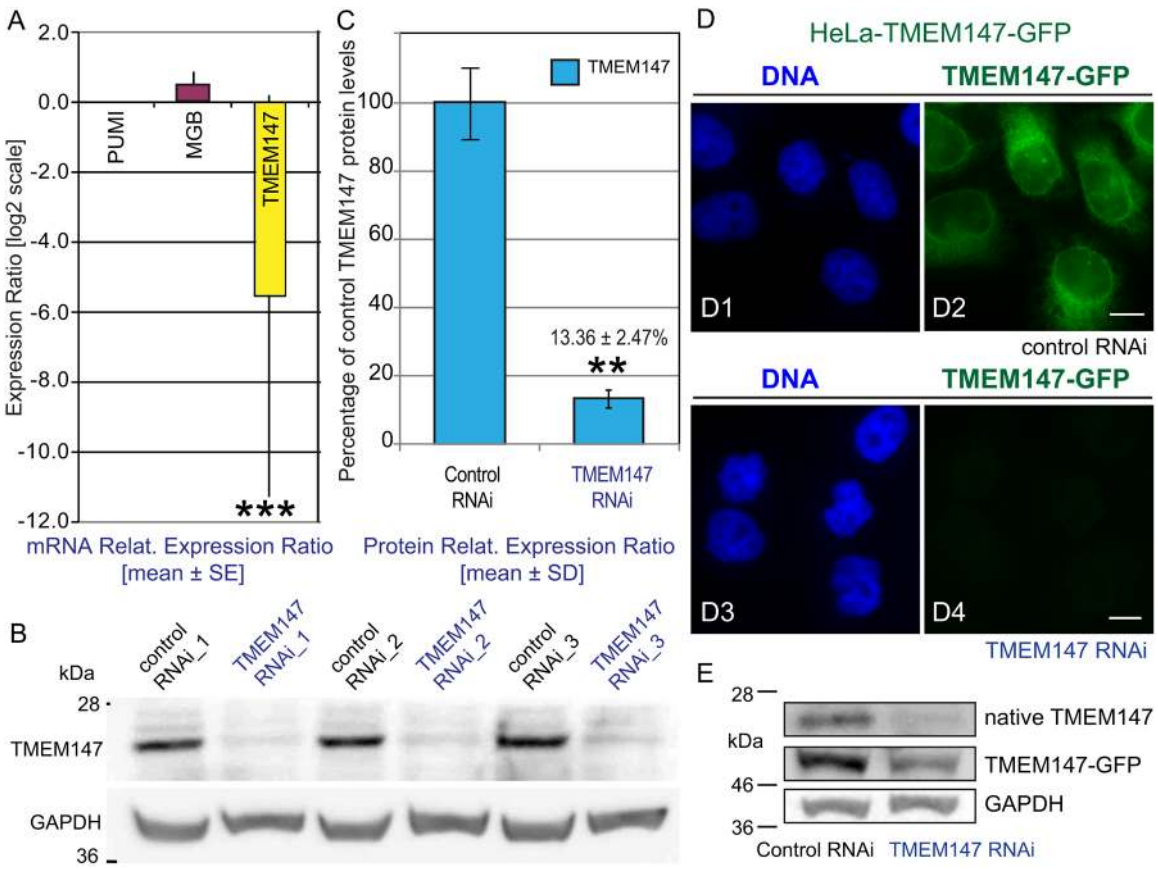

Fig. 2. Confirmation and quantification of silencing of *TMEM147*. (A) Efficiency of *TMEM147*-specific silencing, assessed by RT-qPCR in three independent experiments, depicts an extremely significant (***P<0.0001) normalized *TMEM147* knockdown in silenced cells down to 2.10±1.87% (mean±s.e.m.), expressed as a ratio to the normalized mean negative control value. *PUM1* housekeeping gene mRNA levels were used for sample normalization and *MGB* as an unrelated control. (B) WB analysis of three sets of independent *TMEM147* silencing experiments in HeLa cells showing drastic reduction of the band corresponding to TMEM147, relative to the corresponding negative control silencing reactions. GAPDH immunoreactivity was used as loading control. (C) Quantification of results in B reveals effective reduction of TMEM147 protein levels (normalized to GAPDH) down to 13.36±2.47% (mean±s.d.) of negative control (100±10.35%), with high statistical significance (**P=0.0011) as assessed by a one-tailed heteroscedastic *t*-test. (D) Loss of GFP signal in the TMEM147–GFP stable cell line, as a proxy for TMEM147–GFP protein levels, upon repetition of *TMEM147* silencing, comparing the negative control silencing regime (D1,D2) and *TMEM147*-specific oligonucleotide (D3,D4). Nuclei were counterstained for DNA with Hoechst (blue; D1,D3), and corresponding GFP fluorescence in the same cells is shown in green (D2,D4). Scale bars: 10 µm. (E) Confirmation by WB analysis of effective silencing in TMEM147–GFP HeLa cell line of both native TMEM147 (top panel) and TMEM147-GFP (middle panel). GADPH served as loading control.

mislocalization of LBR, with partitioning of LBR signal to both INM and ER membranes specifically in *TMEM147*-silenced cells (*TMEM147* silencing led to 6.0-fold increased frequency of cells with LBR-positive staining in the ER compared to negative control cells, P<0.0001) (see Fig. 4C,D for representative images; Movie 1 for animation; Table S1 for quantification). Taken together, our analyses suggest that not only does loss of TMEM147 negatively impact LBR production, but it also results in the loss of correct targeting of the residual LBR to the INM and its enhanced mislocalization to the ER. Furthermore, the diminution of LBR levels at the INM is accompanied by chromatin decondensation and a change in nuclear shape.

TMEM147 and LBR proteins physically interact and the C-terminus of LBR is essential for this interaction

Prompted by the observed impact of TMEM147 on LBR protein levels and intracellular targeting, we next investigated, by performing co-immunoprecipitation (co-IP) experiments, whether the two proteins also physically interact. First, conducting IP with an anti-GFP antibody in extracts from the HeLa-TMEM147-GFP or a HeLa-GFP-only stable cell line resulted in the co-selection and detection of endogenous LBR specifically from HeLa-TMEM147-GFP cells, excluding unspecific binding of antibody or GFP to LBR (Fig. 5A, compare lanes c and d). Second, additional IP analyses in HeLa-TMEM147-GFP or HeLa-GFP-only cells that were concurrently transiently transfected with FLAG-tagged full-length LBR detected FLAG–LBR specifically in the bound fraction of TMEM147–GFP samples (Fig. 5B, compare lanes c and f). Thus, these experiments confirm a protein–protein interaction between TMEM147 and LBR and, together with the silencing results, imply a functional interaction between the two proteins.

As mentioned in the Introduction, LBR protein displays a modular organization with involvement of its nucleoplasmic N-terminal domain in chromatin binding and organization at the nuclear periphery, and implication of its membrane-spanning C-terminus in cellular cholesterol biosynthesis. This modular structure thus reflects distinct cellular functions of LBR. To probe the functional association between TMEM147 and LBR, we conducted *TMEM147*-silencing experiments using, in parallel, both wild-type HeLa cells and a stable cell line expressing a GFP-tagged truncated version of LBR, consisting of its full N-terminus plus its first transmembrane domain, HeLa-LBR$_{238}$-GFP (Fig. 6A1; cell line

Journal of Cell Science (2020) 133, jcs245357. doi:10.1242/jcs.245357

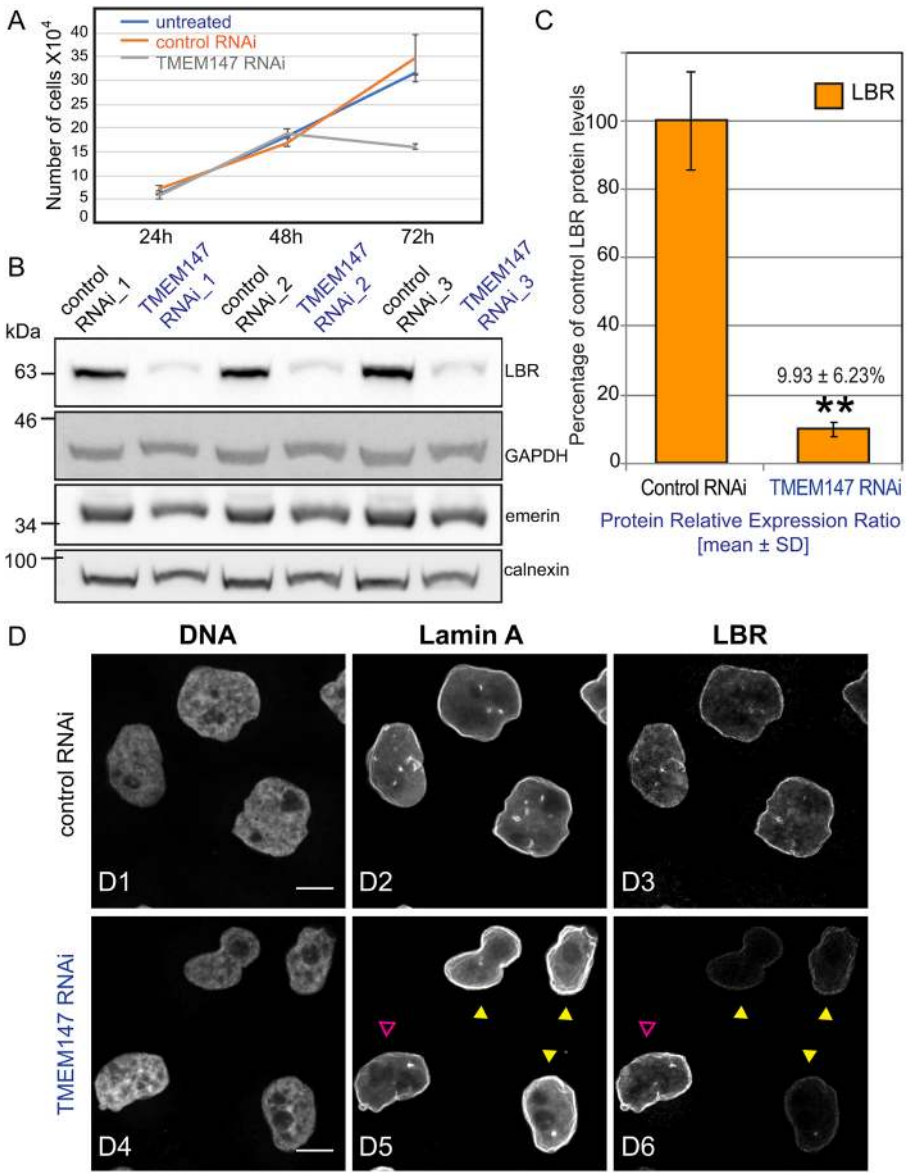

Fig. 3. *TMEM147* silencing results in concurrent significant reduction of LBR protein levels. (A) Growth curves comparing cultures of untreated, control-silenced and *TMEM147*-silenced HeLa cells, seeded in a 24-well plate from an identical number of starting cells (7600) and monitored for 72 h. Cultures were seeded in triplicate, and duplicate measurements were taken from each culture at each time point. Values represent means and bars denote standard deviation of the three experiments, showing a sharp decline in cell numbers in *TMEM147*-silenced cells over time. (B) WB analysis of three sets of independent *TMEM147* silencing experiments in HeLa cells (the same as in Fig. 2A) showing a very large reduction of the band representing LBR, relative to the corresponding negative control silencing reactions. For comparison and as specificity controls, immunoreactivity to INM protein emerin is shown (no change), and to ER integral folding chaperone calnexin (no change). GAPDH immunoreactivity is shown as a loading control. (C) Quantification of results in B determines a reduction of LBR protein levels (normalized to GAPDH) down to 9.93±6.23% (mean±s.d.) of negative control (100±14.35%). The difference is very significant (**P=0.0065), as assessed by two-tailed unpaired t-test with Welch's correction. (D1–D6) Representative examples of maximum intensity projection images by confocal microscopy of nuclei of control-silenced cells labeled for DNA (Hoechst; D1), lamin A as a marker of INM (D2) and LBR (D3), compared with equivalent *TMEM147*-silenced cells (D4,D5,D6). In *TMEM147*-silenced cells, LBR is hardly detectable in the INM (yellow arrowheads in panels D5,D6) (notice one non-silenced cell, indicated with a magenta arrowhead), while lamin A is essentially unaffected. Imaging of different panels was conducted using the same acquisition parameters to allow direct comparison. Scale bars: 10 µm. See also Fig. S1.

by Ellenberg et al., 1997). In these experiments, we assessed and compared the fate of both the endogenous, full-length LBR and the N-terminal LBR_{238}–GFP construct, upon *TMEM147* silencing. Owing to their difference in mass, the two forms of LBR can be distinguished in WB analysis with the anti-LBR antibody, while the truncated form is moreover uniquely detectable with anti-GFP antibody (Fig. S3A,B). As expected, *TMEM147* silencing (22.60±6.81% of negative control levels, P=0.0025; mean±s.d.) produced a robust reduction of endogenous LBR protein (12.77±11.58% of negative control levels, P=0.045) (Fig. 6A2,A3). In contrast, the signal detected for LBR_{238}–GFP either with anti-LBR or anti-GFP antibodies upon *TMEM147* silencing exhibited modest reductions relative to control levels (96.39±41.78% and 77.12±18.10%, respectively) that were not statistically significant (Fig. 6A2,A3). This indicated that the observed stability and persistence of the N-terminal truncated LBR, which contrasted with the drastic reduction of the full-length LBR, likely stemmed from a requirement of the LBR C-terminus for the effect of TMEM147 on LBR protein levels to be manifested. We note, however, the lack of LBR promoter elements driving the expression of LBR238–GFP in the stable cell line, which would explain the lack of effect if regulation was only at the transcriptional level.

We, therefore, next directly addressed the interaction between the two proteins. We designed two overlapping truncated, tagged versions of LBR: LBR_{372}–GFP (the 'N-terminal construct' encompassing the first 372 amino acids of LBR) and $LBR_{209\text{-}615}$–GFP (the 'C-terminal construct" containing amino acids 209–615) and also employed full-length LBR–GFP as a positive control for TMEM147–LBR interaction (Fig. 6B1). Upon transient transfection in HeLa cells, all three constructs localized appropriately to the nuclear rim, with some partitioning to the ER, likely due to overexpression (Fig. 6B2–B4). We conducted IP experiments with anti-GFP beads, immobilizing the GFP-tagged N-terminal, C-terminal or full-length LBR as bait and screened for the presence of endogenous TMEM147 in the bound fractions. We found that, compared to binding of TMEM147 to the full-length LBR–GFP, the binding to the C-terminal construct appeared equally strong, whereas binding to the N-terminal construct was very markedly reduced (Fig. 6B5, compare bound TMEM147 signals in lanes c, f and i). In agreement, the LBR_{238}–GFP N-terminal

Journal of Cell Science (2020) 133, jcs245357. doi:10.1242/jcs.245357

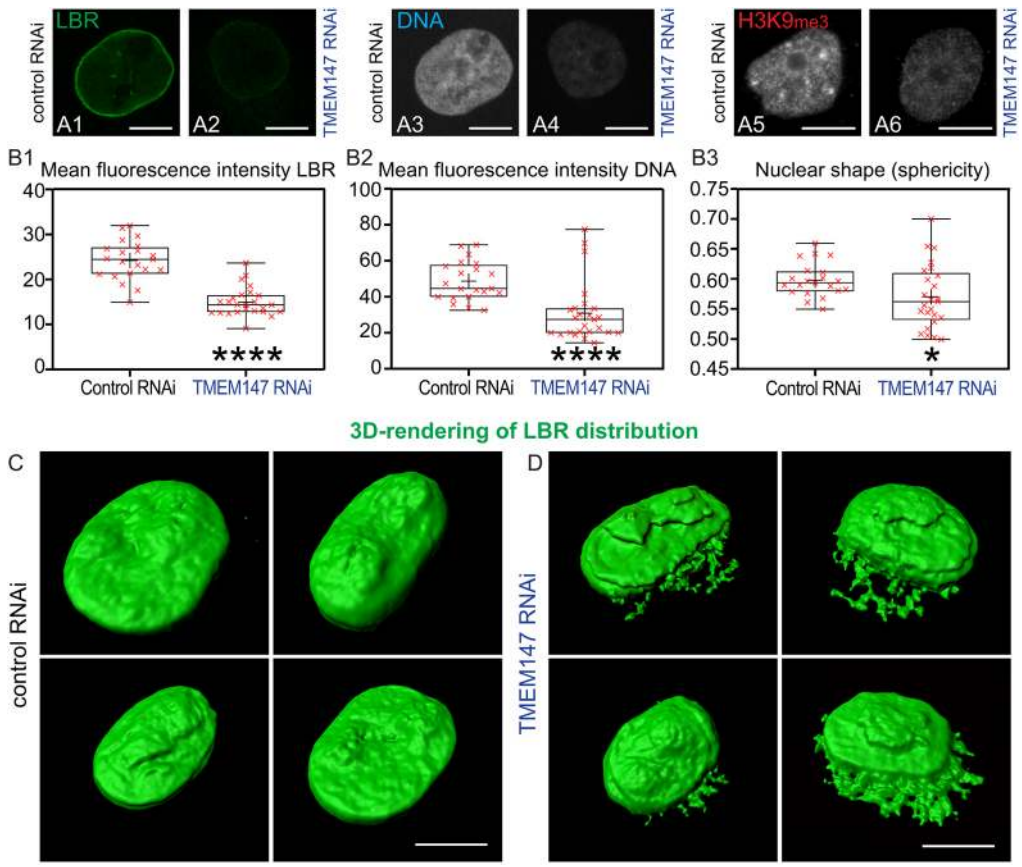

Fig. 4. Further morphometric analysis of LBR changes upon *TMEM147* silencing. (A1,A2) Representative single confocal image of LBR labeling of INM from control-silenced HeLa cell (A1) and loss of LBR labeling in *TMEM147*-silenced HeLa cell (A2). (A3,A4) Maximal projection imaging of stacks of optical sections of the same cells as in A1,A2, respectively, showing drastic reduction of Hoechst labeling of chromatin upon *TMEM147* silencing. (A5,A6) Representative images by widefield microcopy showing clear reduction of H3K9me3 heterochromatin upon *TMEM147*-silencing. Scale bars: 10 µm. (B1) Box-and-whisker plot analysis showing the distribution of all green mean fluorescence intensity (MFI) values for LBR labeling of confocal stacks from four independent silencing experiments for a total of 103 cells (n=55 control silencing, n=48 *TMEM147* siRNA). Mean value marked with a cross (+). Median value of fluorescence intensity of LBR in *TMEM147* siRNA was 14.34 compared to 24.44 units for negative control. MANOVA revealed significant overall difference between silencing and control treatment in LBR signal intensity (****P<0.0001), additionally Mann–Whitney U-test with FDR correction (Q=5%) reported the difference in LBR MFI as an extremely significant discovery (q=0.0002). (B2) Corresponding box-and-whisker plot analysis of the same cells as in B1, exhibiting drastic reduction of Hoechst incorporation, indicative of loss of chromatin compaction in *TMEM147*-silenced cells. Median value of MFI for Hoechst in *TMEM147* siRNA was 27.45 vs 44.66 units for negative control. MANOVA revealed significant overall difference between silencing and control treatment in Hoechst signal intensity (****P<0.0001), additionally Mann–Whitney U-test with FDR correction (Q=5%) reported the difference in Hoechst MFI as extremely significant (q=0.0002). (B3) Box-and-whisker plot analysis of the same cells as in B1 and B2, presenting a small but statistically significant difference in nuclear shape (sphericity quantified in arbitrary units in the whisker plot, as defined by the Imaris algorithm) between control- and *TMEM147*-silenced treatments. Median value of *TMEM147* siRNA was 0.5621 units compared to 0.5937 for negative control [MANOVA *P<0.05 and Mann–Whitney U-test with FDR correction (Q=5%, q=0.0218)]. In all box-and-whisker plots, whiskers indicate minimum to maximum, boxes indicate 25th to 75th percentile, and the central line indicates the median. (C,D) Collections of images of 3D-rendering (Imaris software) of optical section stacks from representative control-silenced (C) and *TMEM147*-silenced cells (D), displaying a clear change in the distribution of LBR signal. Pronounced decoration of additional, ER-bound LBR is detected in *TMEM147*-silenced cells in comparison with control cells displaying the more typical targeting of LBR to the NE. For illustrative purposes, the displays were generated with the same color intensity, not reflecting the profound changes in fluorescence intensity of LBR labeling, as quantified in B1. See also Movie 1. Scale bars: 10 µm.

construct, used in Fig. 6A1–A3, was also unable to bind the native TMEM147, as was the GFP-only bait, used as a negative control (Fig. S3C). These results seem consistent with a protein interaction of TMEM147 with the C-terminus of LBR, and in agreement with the likely topology and orientation of LBR in the INM. Taken together, the results suggest that this interaction at the C-terminus of LBR is the basis of the functional interaction between the two proteins.

Silencing of TMEM147 impacts cellular cholesterol homeostasis

On the basis of our findings that there is a physical and functional interaction between TMEM147 and the C-terminus of LBR, known to exhibit essential C14-sterol reducing activity in cellular cholesterol synthesis, we then investigated whether knockdown of TMEM147 may also impact other key sterol reductases in the same pathway.

Interestingly, quantitative WB analysis of protein levels of 7-dehydrocholesterol reductase DHCR7, the sterol reductase catalyzing the ultimate step in cholesterol biosynthesis and localized, similar to TMEM147, at both ER and the INM (Koczok et al., 2019), revealed that it, too, showed significant reduction to only 32.78±7.98% (mean±s.d.) of control levels specifically upon *TMEM147* silencing in HeLa cells (P=0.026) (Fig. 7A,B). Repetition of these experiments with the stable HeLa TMEM147-GFP cells confirmed similar reductions (Fig. 7A and see legend).

This finding was supported by our additional discovery that DHCR7 was one of the proteins identified as interacting with

Journal of Cell Science (2020) 133, jcs245357. doi:10.1242/jcs.245357

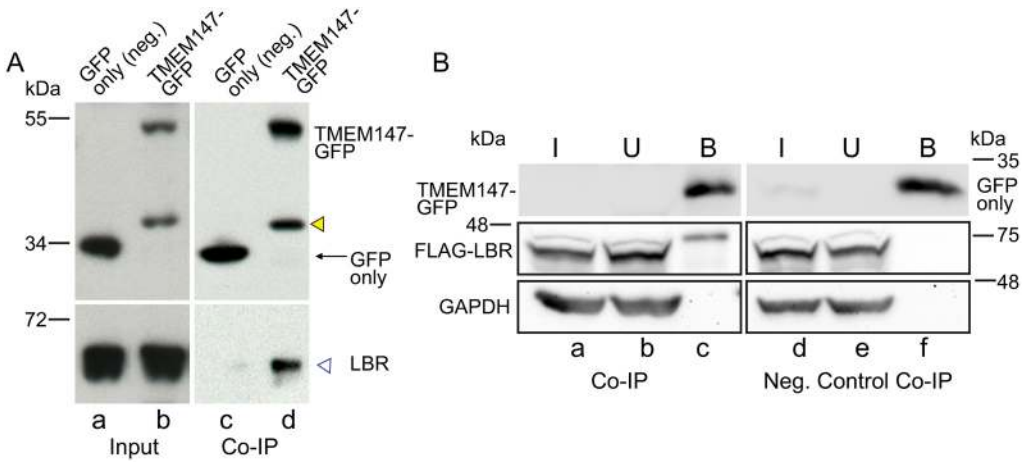

Fig. 5. TMEM147 and LBR proteins interact. (A) The TMEM147–GFP HeLa stable cell line (lanes a,c) or a GFP–only stable line (lanes b,d) were subjected to IP, using anti-GFP beads. Input and GFP-bound fractions were analyzed by WB. Only TMEM147–GFP co-immunoprecipitated the native LBR protein (lane d), while GFP-only, used as a negative control, did not give a signal (lane c). A GFP-containing additional band (lanes b, d), corresponding to an internal translation initiation product, is indicated by a yellow arrowhead. (B) The TMEM147–GFP HeLa stable cell line (left panel) or a GFP-only stable line (right panel) were transiently transfected with a plasmid expressing FLAG–LBR and subjected to IP, using anti-GFP beads. Input, unbound and bound fractions were analyzed by WB. The presence of FLAG–LBR was detected uniquely in the GFP-bound fraction of TMEM147–GFP cells (lane c) but not of GFP-only expressing cells (lane f). I, input; U, unbound fraction/supernatant; B, bound fraction.

TMEM147–GFP by anti-GFP IP, followed by liquid chromatography coupled with tandem mass spectrometry (Fig. S4). In this proteomic analysis, LBR came up as another enriched hit, consistent with our other results, as did the known TMEM147-interacting proteins nicalin and NOMO (Dettmer et al., 2010), validating the analysis (Fig. S4). Thus, TMEM147 and DHCR7 physically interact, and, similar to what is seen for LBR, DHCR7 protein levels are significantly reduced in the absence of TMEM147. TM7SF2, a second key C14 sterol reductase catalyzing the NADPH-dependent reduction earlier in the cholesterol biosynthetic pathway, was also identified as an interacting protein but, in the absence of a reliable antibody, we were unable to validate this further.

We extended our analysis by assessing whether *TMEM147* silencing affected transcription levels of *LBR*, *DHCR7* and *TM7SF2*. Quantification by RT-qPCR indicated that, upon *TMEM147* silencing, there was a clear concurrent reduction of gene expression for both *LBR* and *DHCR7* (Fig. 7C; $P<0.001$ for both *LBR* and *DCHR7*), consistent with the reductions already identified at protein level and the corresponding protein–protein interactions between TMEM147 and these key reductases. In contrast, the level of mRNA for the reductase *TM7SF2* remained essentially unchanged (Fig. 7C). We repeated a quantitative analysis of *TMEM147*, *LBR*, *DHCR7* and *TM7SF2* expression levels, this time from cells grown in parallel in either complete or lipid-restrictive medium (no serum) (Fig. S5). We found *LBR* to be constitutively expressed and unresponsive to lipid starvation (Fig. S5B), in agreement with previous reports (Tsai et al., 2016) and the same applied to the expression of *TMEM147* (Fig. S5A). Furthermore, we observed that negative control cells (as previously reported by Bennati et al., 2008 and Tsai et al., 2016) but also *TMEM147*-silenced (thus *LBR*-downregulated) cells upregulated *TM7SF2* under lipid restriction (Fig. S5C). Interestingly, we detected an even stronger upregulation of *DHCR7* under lipid restriction, and this response was also directly correlated with *TMEM147*/*LBR* expression (Fig. S5D).

Overall, the interconnection found between TMEM147 and both LBR and DHCR7 was remarkable and raised the possibility of a resulting impact of TMEM147 depletion on cellular cholesterol biosynthesis. We thus next employed a full lipidomic analysis to directly measure lipids, including total cellular cholesterol and cholesteryl esters and also quantify the cholesteryl ester species profile (Table S2). We conducted a multivariate analysis of the lipidomics data; a principal component analysis (PCA) of the cellular lipidome (Fig. S6A) indicated that *TMEM147*-silenced cells separated from the control-silenced and untreated cells along the first principal component. Using the loadings plot, we identified that cholesterol and cholesteryl esters (CE) were among the most significant features that drive this separation (Fig. S6B). Surprisingly, total free cholesterol cellular levels in *TMEM147*-silenced cells exhibited a small but significant increase (by 13.4%) when compared with negative control cells (Fig. 7D). Specifically, free cholesterol represented 16.36±0.45 mol% in *TMEM147*-silenced cells vs 14.43±0.16 in negative control ($P<0.05$; mean± s.d.) (Fig. 7D). At the same time, total levels of cholesteryl esters (CEs) were greatly reduced, by 40.5% (5.80±1.68 mol% in *TMEM147*-silenced cells versus 9.74±1.83 compared to negative control cells; $P=0.05$) (Fig. 7D). In addition, quantitation of the full spectrum of lipid species in CEs displayed *TMEM147* silencing-specific alterations (both decreases and increases) in several lipid species (Fig. S6C) with decreases in saturated and short lipid species and increases in several polyunsaturated long fatty-acyl chains of the esterified cholesterol (Fig. S6C).

CEs, as the intracellular storage forms of excess cholesterol, are of central importance to cholesterol homeostasis, and their formation is a measure of the availability of cellular free cholesterol (Luo et al., 2020); reduced CE levels would be consistent with downregulation of sterol reductase activity in *TMEM147*-silenced cells. At the same time, levels of total free cellular cholesterol in *TMEM147*-silenced cells, which were found to be modestly increased in our experiments, represent the contribution of both cellular synthesis as well as that of cholesterol uptake from the growth medium. To specifically determine the contribution of cholesterol uptake in the different cell groups, we therefore conducted cholesterol uptake assays using fluorescently labeled cholesterol, comparing negative control and *TMEM147*-silenced cells under different growth conditions. Cells were grown, in parallel, in complete or lipid-

Journal of Cell Science (2020) 133, jcs245357. doi:10.1242/jcs.245357

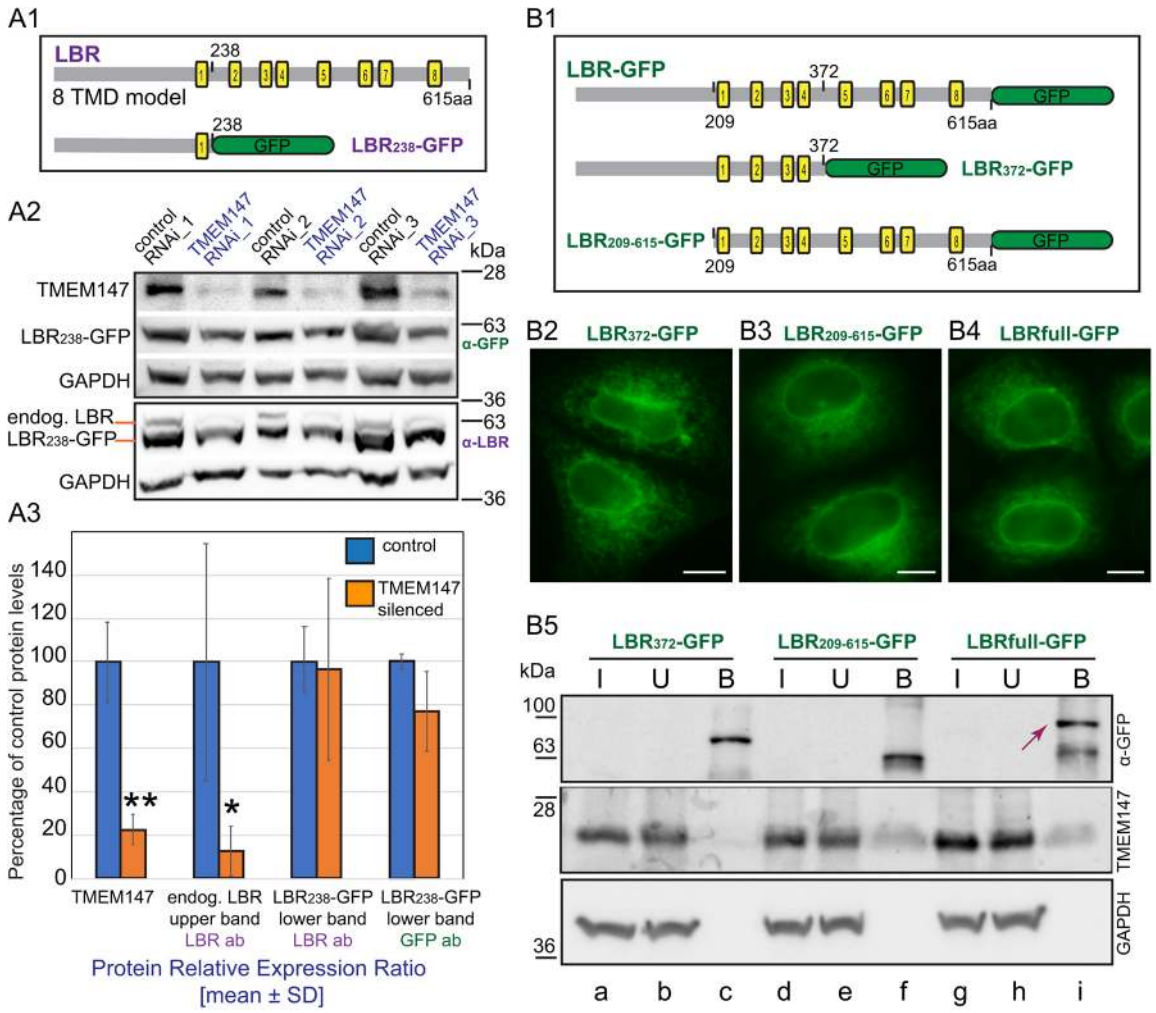

Fig. 6. The C-terminus of LBR is essential for its interaction with TMEM147. (A1) Model of an eight transmembrane domain (TMD) organization of LBR protein; yellow blocks correspond to predicted TMDs (based on LBR transmembrane helix prediction at Uniprot). Below, the structure of a C-terminally truncated construct of LBR containing the first 238 aa fused C-terminally with GFP, as expressed in a stable LBR238-GFP HeLa cell line used in the experiments presented in panels A2 and A3. (A2) WB analysis of three sets of independent *TMEM147* silencing experiments in the LBR_{238}–GFP stable HeLa cell line with the top panel confirming efficient depletion of native TMEM147 protein. Probing with anti-GFP antibody, specifically detecting the GFP-tagged N-terminal truncated version of LBR_{238}-GFP protein, reveals a modest reduction of the band corresponding to LBR_{238}–GFP relative to the equivalent negative control silencing reactions. GAPDH immunoreactivity in the same blots (third panel) was used as loading control. Application of anti-LBR antibody in parallel (fourth panel) allows the detection of both the endogenous full-length LBR (upper band, orange position mark) and LBR_{238}–GFP (lower band, orange mark) (see also Fig. S3A); knockdown of full-length LBR appears more pronounced than reduction of LBR_{238}–GFP signal. GAPDH immunoreactivity in the same blot (bottom) is shown as a loading control. (A3) Quantification of results in A2 confirming effective reduction of TMEM147 protein levels (normalized to GAPDH) down to 22.60±6.81% (mean±s.d.) of negative control (**P=0.002). Furthermore, comparison of endogenous LBR levels (upper band in bottom panel in A2) shows a drastic reduction in *TMEM147*-silenced cells, consistent with our other findings (Fig. 3, Figs S1 and S2), to 12.77±11.58% of negative control (*P=0.04). In contrast, the truncated construct LBR238-GFP (lower band in bottom panel in A2) shows small and statistically non-significant reduction upon *TMEM147* silencing, as revealed both by LBR and GFP immunoreactivity [96.39±41.78% (P=0.7) and 77.12±18.10% (P=0.06), respectively]. The impact of *TMEM147* silencing on protein levels was assessed without assuming a consistent s.d. and using individual two-tailed unpaired *t*-tests for TMEM147, the upper and lower LBR bands and GFP values, normalized to GAPDH. (B1) Schematic summarizing the 'N-terminal' (LBR_{372}–GFP) and 'C-terminal' constructs ($LBR_{209\text{-}615}$–GFP), both fused C-terminally with GFP, as compared to full-length LBR. These three constructs were used for transient transfections in the experiments shown in B2–B5. (B2–B4) Representative images of the expression of LBR_{372}–GFP, $LBR_{209\text{-}615}$–GFP and full-length LBR–GFP in HeLa cells (green GFP fluorescence), displaying appropriate localization at the NE and extending to the ER (possibly due to overexpression). Scale bars: 10 µm. (B5) HeLa cells transiently transfected in parallel with plasmids expressing LBR_{372}–GFP, or $LBR_{209\text{-}615}$–GFP or full-length LBR–GFP, were subjected to IP using anti-GFP beads. Input (I), unbound (U) and bound (B) fractions were analyzed by WB to compare the presence of native TMEM147 in each case. Top panel confirms binding of GFP-tagged versions of LBR in the bound fractions as bait (full-length LBR-GFP indicated by red arrow). Middle panel indicates co-selection of native TMEM147 in the bound fractions of full-length LBR–GFP (lane f) and of the bound fraction of C-terminal construct $LBR_{209\text{-}615}$–GFP (lane i) but only a barely detectable signal in the bound fraction of N-terminal construct LBR_{372}–GFP (lane c). Bottom panel displays GAPDH immunoreactivity as a loading control. This result was representative of multiple repetitions of the experiment. See also Fig. S3C for extra results and negative controls.

restrictive medium (no serum) or in the presence of cholesterol transport inhibitor U-18666A (as a positive control of increased uptake) (Fig. 7E). In all conditions tested, normalized cholesterol uptake was markedly and significantly increased in *TMEM147*-silenced cells in comparison with negative controls. In particular, uptake was doubled in restrictive medium conditions relative to negative control, and in complete medium it increased by 2.3-fold (Fig. 7E). Increased uptake, to counteract impaired cellular

Journal of Cell Science (2020) 133, jcs245357. doi:10.1242/jcs.245357

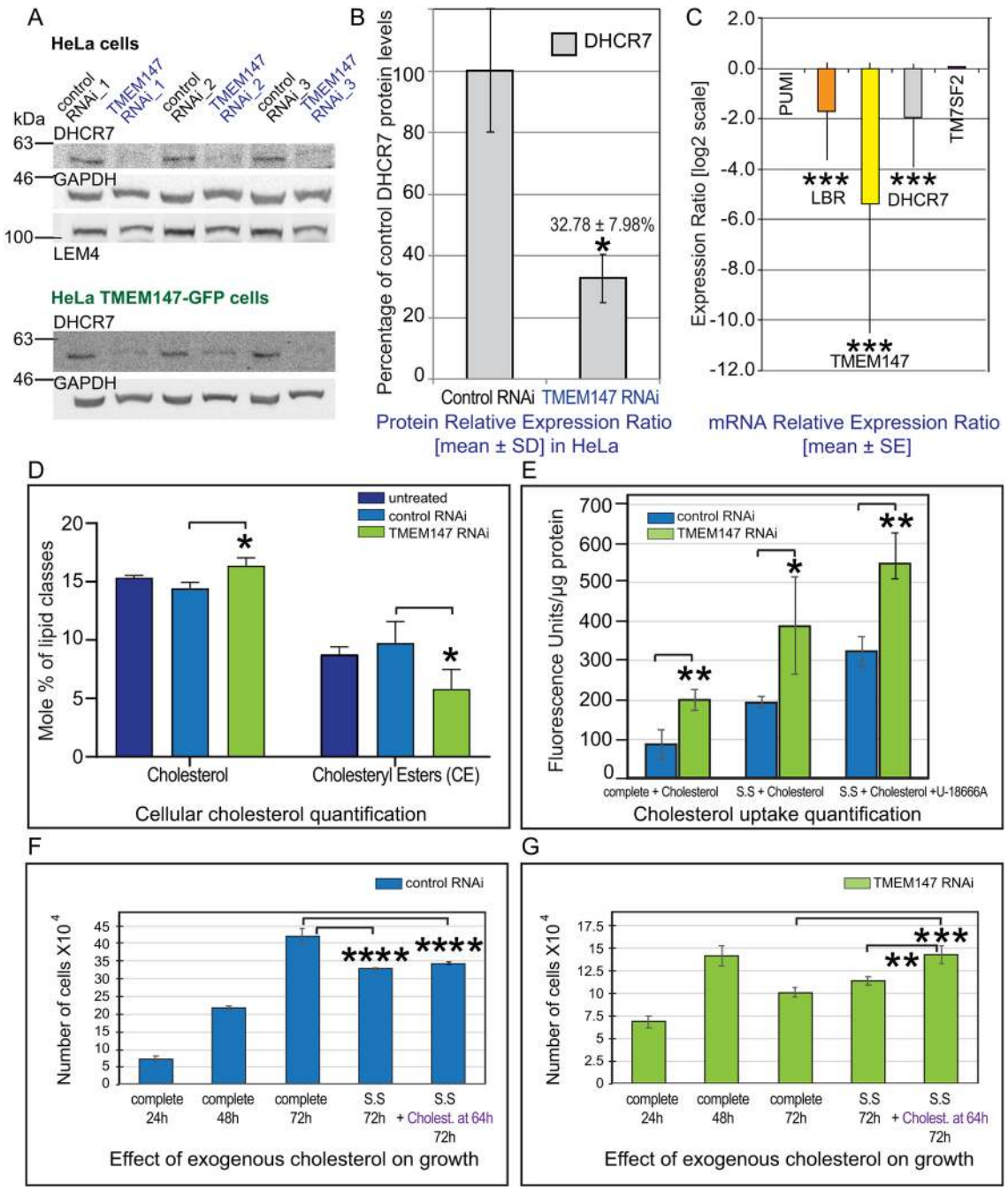

Fig. 7. See next page for legend.

biosynthesis due to the reduction of both LBR and DHCR7, would explain the maintenance of free cholesterol levels in *TMEM147*-silenced cells grown in non-restrictive media (Fig. 7D).

Consistent with these findings was the effect of cholesterol rescue in growth assays. Control and *TMEM147*-silenced cells were grown either in complete medium or in complete medium followed by a 24-h lipid restriction (no serum) either on its own or in combination with exogenous cholesterol, and cell viability was monitored at different time points (Fig. 7F,G). Addition of exogenous cholesterol for the last 8 h during the 24-h lipid restriction rescued growth and restored it by 72 h to the same levels [(14.27±0.95)×10^4 cells] as those observed for cells at 48 h in complete medium [(14.06±1.13)×10^4 cells], specifically in *TMEM147* silencing (Fig. 7G); in comparison, equivalent *TMEM147*-silenced cells at 72 h without cholesterol showed the typical drastic reduction in viability [(11.35±0.48)×10^4 *TMEM147*-silenced cells with serum starvation at 72 h versus (14.3±0.95)×10^4 cells with serum starvation plus cholesterol at 72 h (P=0.0046), or (10.10±0.48)×10^4 *TMEM147*-silenced cells in complete medium at 72 h compared again with cells in the presence of cholesterol (P=0.0003)] (Fig. 7G). Cholesterol addition had only a very modest positive effect on lipid-restricted negative control cells (Fig. 7F). Interestingly, we observed that in *TMEM147*-silenced cells that were already growth affected at 48 h, subsequent lipid depletion at 48 h had essentially no additional aggravating impact compared to the rapid growth decline manifested by 72 h in complete medium, in contrast to control

Journal of Cell Science (2020) 133, jcs245357. doi:10.1242/jcs.245357

Fig. 7. Silencing of *TMEM147* impacts cholesterol metabolism in HeLa cells. (A) WB analysis of three sets of independent *TMEM147* silencing experiments in HeLa cells (top set) or TMEM147–GFP HeLa cells (bottom set) showing a large decrease of the band corresponding to C14-sterol reductase DHCR7, relative to the corresponding negative control samples. Immunoreactivity to the ER integral protein LEM4 was used as negative control and GAPDH immunoreactivity as loading control. (B) Quantification of results in A showing a reduction of DHCR7 protein levels (normalized to GAPDH) in *TMEM147*-silenced cells down to 32.78±7.98% (mean±s.d.) of negative control (100±20.01%), with statistical significance (**P*=0.026), as assessed by a two-tailed heteroscedastic *t*-test (Microsoft Excel). The corresponding value for TMEM147–GFP HeLa cells in A was down to 36.80±19.25% of negative control value (**P*=0.04). (C) Assessment by RT-qPCR in three independent experiments of *LBR*, *DHCR7* and *TM7SF2* mRNA levels in *TMEM147*-silenced cells showing that there is a highly statistically significant co-ordinated downregulation of *LBR* and *DHCR7* (****P*<0.0001), but no change of *TM7SF2*, expressed as a ratio to the normalized mean control value. Specifically, *LBR* mRNA levels are down by 3.29 times or to 30.40±26.08% (mean±s.e.m.) and *DHCR7* by 3.84 times or to 26.0±24.04% of negative control levels. *TM7SF2* is essentially unchanged compared to negative control (increase by a factor of 1.058 and non-significant *P*=0.09). *L19* and *PUM1* were used as reference genes for normalization. Error bars correspond to the s.e.m. of triplicate analysis. (D) Total free cellular cholesterol levels and total cholesteryl ester (CE) levels, as determined by LC/MS analysis, comparing untreated cells, negative control silenced and *TMEM147*-silenced cells in three independent experiments. Changes in cholesterol or CE, for a comparison of *TMEM147*-silenced to control-silenced cells, were significant as assessed by multiple *t*-test with multiple testing correction based on FDR correction (Q=5%). Specifically, free cholesterol in *TMEM147*-silenced cells was increased to 16.36±0.45 mol% vs 14.43±0.16 in negative control cells (q=0.017). Total CE were reduced in *TMEM147*-silenced cells to 5.80±1.68 mol% vs 9.74±1.83 in negative control cells (q=0.0267). Results are mean±s.d. (E) Cholesterol uptake assay comparing negative control silenced and *TMEM147*-silenced cells in three independent experiments with cells grown in complete medium, or serum-free medium or serum-free medium in the presence of 1 µM cholesterol transport inhibitor U-18666A. Emission of fluorescently labeled cholesterol was normalized to protein content in each well and background fluorescence was subtracted from equivalent measurements per condition without cholesterol. Changes in all cases were significant, as assessed by multiple *t*-test with multiple testing correction and FDR correction (Q=5%). In particular, cholesterol uptake in *TMEM147*-silenced cells in complete medium was increased to 199.39±26.14 emission units/µg protein vs 86.58±35.65 (mean±s.d.) in negative control cells (**q=0.006); in *TMEM147*-silenced cells in restrictive, serum-starvation (S.S) medium, it was increased to 388.43 ±123.93 vs 193.50±14.17 (*q=0.019); in restrictive medium plus transport inhibitor to 548.80±56.17 vs 324.22±36.85 (**q=0.005). (F,G) Assessment of growth in three independent experiments, comparing cultures of control-silenced (F) and *TMEM147*-silenced cells (G), seeded in identical numbers and monitored for 72 h (triplicate measurements/time point). Cells were grown in complete medium for 72 h, or in complete medium for 48 h and then with serum starvation (S.S) until 72 h, or in complete medium for 48 h and with serum starvation until 72 h with addition of cholesterol at 64 h. Values represent means±s.d. Addition of cholesterol in lipid restricted *TMEM147*-silenced cells (G) restores growth at 72 h to values similar to those in cells at 48 h in complete medium and this does not happen in the absence of cholesterol [(11.35±0.48)×10^4 *TMEM147*-silenced cells with S.S at 72 h vs (14.3±0.95)×10^4 with S.S plus cholesterol at 72 h (***P*=0.0046), or (10.10 ±0.48)×10^4 *TMEM147*-silenced cells in complete medium at 72 h vs, again, cells with S.S and cholesterol addition (****P*=0.0003)]. In F, differences between cell numbers at 72 h in complete medium vs S.S without cholesterol or vs S.S with cholesterol addition remain significantly reduced (*****P*<0.0001 for both comparisons), indicating that addition of cholesterol does not improve cell viability.

cells (Fig. 7F,G), suggesting that the detrimental impact of *TMEM147* silencing on growth was severe and already developing in complete medium (see also Fig. 3A). This is different to the observations of Tsai et al. (2016), where decreased viability of LBR-knockout cells occurred under lipid restriction only, and likely underlines the more severe phenotypes resulting from TMEM147-induced depletion of both LBR and DHCR7.

In conclusion, our work provides evidence to indicate a role for TMEM147 as a novel functional modulator of cholesterol homeostasis in cells.

DISCUSSION

Previously described roles for TMEM147 included membrane complex stabilization (Dettmer et al., 2010), acetylcholine receptor trafficking (Rosemond et al., 2011) and NF-κB activation (Ota et al., 2019). In this work, we present evidence for physical and functional interactions between the ER and INM transmembrane protein TMEM147 and the well-characterized LBR protein, which, through its modular structure, serves both as a heterochromatin organizer at the nuclear lamina and a sterol reductase in the late steps of cholesterol biosynthesis. We discovered that downregulation of *TMEM147* in human cells induces a sharp reduction in LBR protein levels and mislocalization of the remaining LBR to the ER at the expense of its typical localization at the INM. Furthermore, we discovered that TMEM147 physically interacts with DHCR7, another key sterol reductase in cholesterol biosynthesis in cells. Interestingly, *LBR* and *DHCR7* exhibit co-ordinated reductions in gene expression upon *TMEM147* knockdown, in contrast with what was seen with the sterol reductase TM7SF2, the gene expression of which appeared to be unaffected by downregulation of *TMEM147*. Consistent with these data on interactions and gene expression, we identified changes in cellular cholesterol and cholesteryl ester levels as well as in cellular cholesterol uptake in *TMEM147*-silenced cells, supporting the idea that TMEM147 functions as an important regulator of cholesterol homeostasis in cells.

Cholesterol is the major sterol in terrestrial vertebrates and critical for normal growth, development and hedgehog signaling in mammals. It is a regulator of membrane fluidity and organization, a key component of lipid rafts in the plasma membrane, and important in myelin formation in nerves (reviewed by Platt et al., 2014). Most mammalian cell types modulate the cholesterol content of their membranes by finely balancing cellular cholesterol biosynthesis, uptake by receptor-mediated endocytosis and export of esterified cholesterol via ABC transporters. Our findings reveal that in the absence of TMEM147 (and consequent depletion in the levels of both LBR and DHCR7), uptake of cholesterol is increased, presumably to counteract the reduction of endogenously produced cholesterol and its cholesteryl esters. Despite increased uptake, changes in cholesterol metabolism may account for the observed cell death at late stages of *TMEM147* silencing, compared to negative control cells, even in the presence of complete medium. Addition of exogenous cholesterol increased cell viability, but we cannot formally exclude additive detrimental effects of TMEM147 silencing contributing to increased cell death rates.

Our finding that *TMEM147* downregulation in HeLa cells, resulting in concomitant downregulation of *LBR* (and *DHCR7*), does not seem to affect gene expression of the reductase TM7SF2, indicates that there are distinct forms of transcriptional regulation for LBR and TM7SF2, even though both proteins are thought to catalyze the same enzymatic step in cholesterol biosynthesis. These results appear in agreement with both the study by Bennati et al., 2008, in which *Tm7sf2*$^{-/-}$ mice had normal LBR protein levels, and the more recent analysis by Tsai et al., 2016, in which primary human cells or cell lines (including HeLa cells) did not show co-ordination of gene expression between *LBR* (constitutively expressed) and *TM7SF2* (sterol-inducible), either under standard conditions or under prolonged lipid starvation. During mouse liver regeneration, TM7SF2 and LBR are again differently modulated and absence of TM7SF2 does not impair cholesterol biosynthesis

Journal of Cell Science (2020) 133, jcs245357. doi:10.1242/jcs.245357

(Bartoli et al., 2016). TM7SF2 and LBR were also found to undergo differential post-translational regulation, with TM7SF2 manisfesting sterol-dependent turnover while LBR remained stable (Capell-Hattam et al., 2020). The unresponsiveness of *TM7SF2* to changes in *LBR* expression, revealed in all of these studies and by our experiments, is somewhat counterintuitive and would challenge the notion that TM7SF2 can compensate for cholesterol biosynthesis in the absence of functional LBR in order to sustain cholesterol levels (Wassif et al., 2007).

We report here both a novel protein–protein interaction between TMEM147 and DHCR7, a co-ordinate gene expression between *LBR* and *DHCR7* in response to *TMEM147* depletion in normal conditions, and an induction of *DHCR7* under lipid restriction that is modulated by *TMEM147*/*LBR* expression. Despite the wealth of studies on DHCR7 as the cause of SLOS, its functional relationship and molecular interactions with LBR have remained relatively obscure. It would appear that TMEM147 as an upstream positive regulator impacts both LBR and DHCR7, affecting their gene expression and protein levels in a molecular mechanism that remains to be investigated. Interestingly, protein interaction data (https://www.ebi.ac.uk/intact/interactors/id:Q9BVK8), include experimental evidence for physical interaction between TMEM147 and the emopamil-binding protein EBP (or D8D7I), a 3-β-hydroxysteroid-δ(8),δ(7) isomerase catalyzing the conversion of δ(8) sterols to their corresponding δ(7) isomers in cholesterol biosynthesis, upstream of DHCR7 (Silve et al., 1996). EBP (also known as D8D78I), like TMEM147 and LBR, localizes to both the ER and the NE, and its mutations impair cholesterol synthesis and cause X-dominant chondrodysplasia punctata with ichthyosis (Braverman et al., 1999; Liu et al., 1999). EBP displays co-ordinate transcription with DHCR7, with which it also forms a bifunctional complex (ChEH, cholesterol-5-6-epoxide hydrolase) (Kedjouar et al., 2004; de Medina et al., 2010), raising the possibility that the pattern of common gene expression of LBR and DHCR7 influenced by TMEM147 may include further enzymes of late cholesterol synthesis steps, like EBP.

Our observation of LBR mislocalization to the ER in the absence of TMEM147 is intriguing and reminiscent of its similar partitioning when the nucleoporin ELYS (also known as AHCTF1) is downregulated (Clever et al., 2012; Mimura et al., 2016). Following its synthesis, LBR diffuses laterally through the ER and the nuclear pore membrane domains, via lateral peripheral channels of the complexes, before becoming anchored at the INM by binding, via its N-terminus, to the nuclear lamina, heterochromatin or other proteins (Ellenberg et al., 1997; Makatsori et al., 2004; Ungricht et al., 2015; Boni et al., 2015; Giannios et al., 2017). The vast majority of steady-state LBR is at the INM, as opposed to the ER (Nikolakaki et al., 2017). Not only does the number of nuclear pore complexes thus appear important, but also INM localization of LBR was found to be inhibited by SR phosphorylation of the N-terminal domain, involving kinases CDK, SRPKs or ELYS protein acting on protein phosphatases (Nikolakaki et al., 1996; Tseng and Chen, 2011; Fukuhara et al., 2006; Mimura et al., 2016). An interesting point of discussion has been whether the ability of LBR to contribute to cholesterol synthesis *in vivo* is conditional on its presence at the NE or the ER (Hoffmann et al., 2007). If LBR localization is indeed critical for its enzymatic activity, then it would appear that interaction between LBR and TMEM147 is essential for INM targeting of LBR. We found that absence of TMEM147 not only caused a drastic decline of LBR protein levels but also an altered diffusional mobility of LBR and its relocation to the ER. This mislocalization of LBR may further contribute to the impact of LBR reduction on cholesterol synthesis.

Other phenotypic effects that we report, upon *TMEM147* silencing and the associated LBR depletion from the NE, were a change in nuclear shape (but not size or surface area) as well as evidence of loss of chromatin compaction. Both of these features (1) are highly consistent with observed effects upon loss of LBR expression in many studies, and (2) were shown to be tightly entwined in cellular physiology. Specifically, in Pelger–Huët syndrome in humans, mutations resulting in truncated and unstable forms of LBR are accompanied by hypolobulated nuclei in granulocytes (Hoffmann et al., 2002), while in ichtyosis in mice, nuclei are ovoid and with 'inverted nuclear organization', that is with heterochromatin masses accumulating internally and non-compacted chromatin at the nuclear periphery (Hoffmann et al., 2007; Shultz et al., 2003). Additionally, it is well documented that in healthy blood granulocyte differentiation in the bone marrow, wild-type LBR is developmentally upregulated as granulopoiesis progresses, relating to both increased nuclear indentation (shaping the characteristic polylobular nuclei) and heterochromatin tethering to the nuclear periphery in mature neutrophils, the main granulocyte cell type (Olins et al., 2008). In myeloid cell line models (human HL-60 and mouse EPRO promyelocytes), correspondingly, the absence of LBR produces profound effects in both nuclear shape and heterochromatin distribution in a dose-dependent manner (Zwerger et al., 2008; Hoffmann et al., 2007; Olins et al., 2010). In the same vein, it was demonstrated that *LBR* knockdown in HeLa cells resulted in redistribution and unfolding of heterochromatin from the INM towards the nucleoplasm (Lukášová et al., 2017). LBR has additionally been proposed as a stimulator of NE growth on the basis of overexpression experiments resulting in NE overproduction, inducing NE invagination and membrane stack formation (Ma et al., 2007).

The evidence linking the generation of nuclear shape with the function of LBR as organizer of underlying heterochromatin is compelling; however, one thought-provoking novel hypothesis, also taking into consideration the question of why there should be a need for cholesterol production specifically at the INM (in addition to the ER), is the idea that cholesterol, becoming readily accessible to the nucleus, may participate in the assembly of nuclear lipid microdomains ('nuclear lipid rafts', in analogy to plasma membrane lipid rafts) that may provide specialized chromatin-anchoring platforms, nucleosome-binding domains, or scaffolds for protein organization or oligomerization (Cascianelli et al., 2008; Codini et al., 2016; Silva et al., 2017; Nikolakaki et al., 2017). This possibility was proposed as an explanation of the unique role of LBR in cholesterol biosynthesis, which cannot be compensated for by the ER sterol reductase TM7SF2, even though both proteins catalyze the same reaction (Nikolakaki et al., 2017). If this were indeed the case, it would provide an intriguing and meaningful framework to reconcile and understand the dual and diverging modular structure and functional role of LBR in both nuclear organization/gene expression and cholesterol biosynthesis. And it would illuminate TMEM147 as a putative upstream functional integrator, via its modulation of LBR, of gene expression and cholesterol homeostasis. Dissecting the molecular mechanism through which the novel physical and functional interaction of TMEM147 with LBR impacts both processes is now essential in order to fully understand their cellular interplay.

MATERIALS AND METHODS

Cell culture and generation of the HeLa-TMEM147-GFP stable cell line

HeLa (Kyoto; K; EMBL) cells were cultured in DMEM containing 10% (v/v) fetal bovine serum (FBS), 2 mM glutamine and 50 U/ml of penicillin/

streptomycin (complete medium) and maintained at 37°C in 5% CO_2. For some experiments, cells were grown in lipid restrictive medium (complete medium without FBS). Cells were regularly tested by PCR and Hoechst 33342 staining to ascertain lack of mycoplasma infection.

The stable HeLa K TMEM147-GFP cell line was generated by transient transfection of pEGFPN1-TMEM147 into HeLa K cells. Expressing cells were selected in the complete medium supplemented with 0.5 mg/ml G418 (Invitrogen) and further enriched by FACS.

The HeLa LBR_{238}–GFP stable cell line, expressing a fusion between the first 238 N-terminal amino acids (aa) of human LBR and a C-terminal in-frame GFP sequence, was a gift from Jan Ellenberg (EMBL Heidelberg, Germany).

RT-qPCR for analysis of gene expression

For relative quantification of mRNA in silencing experiments, RT-qPCR was conducted on the CFX96 Real-Time PCR system (Bio-Rad) in 96-well plates and primers specific for either human *TMEM147* (for, 5′-GTACAACGCCTTCTGGAAATG-3′; rev, 5′-ATGCTGTTCTTGGCCACTTT-3′), *LBR* (for, 5′-GGTCGACCACCTAAAAGTGC-3′; rev, 5′-CCCCATTATATCTGCTGATGC-3′), *DHCR7* (for, 5′-CCCAGCTCTATACCTTGTGG-3′; rev, 5′-CCAGAGCAGGTGCGTGAGGAG-3′) or *TM7SF2* (for, 5′-AACTCAGGCAATCCGATTTACG-3′; rev, 5′-GGGTCGCAGTTCACAGAAATA-3′). Melting curve analysis was performed to determine the amplification specificity. Three independent experiments were conducted, and each included two no-template controls; all samples were repeated in triplicate reactions. For data normalization, expression of ribosomal protein L19 (*RPL19*) and pumilio homolog 1 transcript variant 2 (*PUM1*) were used as reference genes and mammaglobin B-2 (*MGB2*) as an unrelated marker (all sequences of PCR primers as per Pantelidou et al., 2007). For statistical analysis of RT-qPCR data, the REST-384© software was used to calculate the relative expression ratio of the different groups and determine the significance of results (Pfaffl et al., 2002; Pantelidou et al., 2007). For the RT-qPCR analysis in Fig. S5, negative control or *TMEM147*-silenced cells were grown in parallel either in complete medium (72 h) or lipid restrictive medium (48 h in complete medium+24 h under serum starvation). The Common Base method was used to allow direct quantitative comparisons across samples (Ganger et al., 2017), combined with statistical evaluation by two-way ANOVA followed by Tukey's post hoc test for multiple comparisons (GraphPad Prism 8.0).

siRNA-mediated silencing

Transfections for RNAi experiments were performed using INTERFERin (Polyplus Transfection) and siRNA oligonucleotides specific for *TMEM147* (oligo#1, 5′-GGCGGCAUCUAUGACUUCATT-3′; oligo#2, 5′-CGCUAUGAUCUGUACCACATT-3′) (Ambion Inc.), at a final concentration of 40 nM and according to the manufacturer's specifications. Negative control was a mock, no-oligo, transfection reaction. Cells were harvested 72 h after addition of siRNAs (96 h for oligo#2) for immunofluorescence (IF), RT-qPCR and western blot (WB) analysis.

SDS-PAGE, quantitative WB and statistical analysis

Protein samples were heated only to 60°C for 10 min to avoid aggregation of TMEM147 (Dettmer et al., 2010). SDS-PAGE was performed on a Mini-Protean II Electrophoresis Cell, WB on a Mini Trans-Blot Transfer Cell (Bio-Rad), using 48 mM Tris-HCl pH 9.2, 39 mM glycine and 20% (v/v) methanol for transfer, and the ECL System (GE Healthcare) with G:BOX (SYNGENE) for visualization. For quantification of protein levels, intensity volumes (area×height) of signals were extracted with ImageJ 1.49n and normalized using same-sample and same-membrane band intensities for the housekeeping protein GAPDH (in triplicate reactions for each independent experiment). GAPDH-normalized protein expression values were subjected to normality tests (GraphPad Prism 8.0) and significance of knockdown for individual protein bands was assessed by corresponding parametric or non-parametric statistical comparisons (Microsoft Excel and GraphPad Prism 8.0) (see figure legends for further details).

Antibodies

A mouse monoclonal antibody against human TMEM147 (NM_001242598.1) had previously been generated and characterized (Dettmer et al., 2010) and was used here at 1:8 dilution for WB. Additional commercial primary antibodies used were as follows: rabbit anti-LBR (E398L) (Abcam ab32535; 1:300 for IF and WB), mouse anti-LAP2β (BD Transduction Laboratories 611000; 1:500 for IF), mouse anti-GAPDH (Santa Cruz Biotechnology sc-32233; 1:500 for WB), mouse anti-FLAG (Sigma-Aldrich F4042; 1:500 for IF and WB), mouse anti-EGFP (Roche 11814460001; 1:1000 for IF and WB), rabbit anti-calnexin (Santa Cruz Biotechnology sc-11397; 1:100 for IF and 1:200 for WB), rabbit anti-emerin (Abcam ab14208; 1:400 for WB), rabbit anti-LEM4 (Asencio et al., 2012; 1:100 for WB), mouse anti-lamin A (Abcam ab8980; 1:500 for IF), rabbit anti-DHCR7 (Origene TA349889; 1:300 for IF), anti-histone H3K9-me3 (Millipore 17-625; 1:500 for IF). Primary antibodies were used in conjunction with appropriate fluorescently labeled Alexa-Fluor secondary antibodies (Thermo Fisher Scientific) for immunofluorescence, or HRP-labeled secondary antibodies (Santa Cruz Biotechnology) for WB. Nuclei were counterstained with Hoechst 33342 (0.5 µg/ml).

Expression plasmid constructs

For expression in HeLa cells, the full length ORF of *TMEM147* was amplified from HeLa K with primer set TMEM147F, 5′-CGCTCGAGATGACCCTGTTTCACTTCGGGAACTG-3′ and TMEM147R, 5′-GCGAATTCCGGAGTGCACATTGACAACGGCGACAT-3′, transferred as an XhoI/*Eco*RI fragment into pEGFP-N1 (Clontech) and transferred as a BglII/KpnI fragment into pFLAG-CMV-2 (Sigma-Aldrich).

An equivalent cloning strategy was followed for generating full-length GFP- and FLAG-tagged LBR constructs for expression in HeLa cells with primer set LBR1-615F, 5′-CGCGCTCGAGATGCCAAGTAGGAAATTTG-3′ and LBR1-615R: 5′-CGCGGAATTCGGTAGATGTATGGAAATA-3′. To clone truncated version LBR_{372}–GFP into pEGFP-N1, oligo LBR1-615F was used in conjunction with LBR1-372R, 5′-CGCGGAATTCGACGGCCAATGAAGAAATCATA-3′. Finally, to generate truncated version $LBR_{209\text{-}615}$–GFP, oligo LBR209-615F, 5′-CGCGCTCGAGTTTGGAGGAGTACCTGGTG-3′ was used in conjunction with LBR1-615R.

Co-IP analysis of protein interactions and LC-MS/MS analysis

HeLa K TMEM147-GFP cell line and HeLa K GFP cell line (negative control), either alone or transiently transfected with FLAG–LBR constructs, were lysed in lysis buffer [20 mM Tris-HCl pH 7.5, 150 mM NaCl, 1% v/v NP40 and 1× Complete™ (a protease inhibitor cocktail by Roche)]. Each of the extracts was incubated with a 10 µl slurry of GFP-Trap_A beads (Chromotek) for 2 h at room temperature. After binding, beads were extensively washed in lysis buffer and bound proteins were eluted from beads using 30 µl SDS-PAGE sample buffer. Samples were heated to 60°C for 10 min and then analyzed by SDS-PAGE, followed by WB.

For the co-IP experiment shown in Fig. S4, proteomic analysis was carried out at the EMBL Heidelberg Proteomics Facility. IP samples (TMEM147-GFP IP as test sample, TMEM129-GFP IP for comparison, and GFP-only IP as negative control) from two independent experiments in parallel (six samples in total) were prepared for MS analysis using the SP3 protocol (Hughes et al., 2019). Peptides were labeled with TMT6plex Isobaric Label Reagent (ThermoFisher), according the manufacturer's instructions, pooled and cleaned up further with an OASIS® HLB µElution Plate (Waters). Offline high pH reversed phase fractionation was carried out on an Agilent 1200 Infinity high-performance liquid chromatography system, equipped with a Gemini C18 column (Phenomenex). MS data acquisition was performed with an UltiMate 3000 RSLC nano LC system (Dionex), fitted with a trapping cartridge (µ-Precolumn C18 PepMap 100) and an analytical column (nanoEase™ M/Z HSS T3 column Waters), directly coupled to an Orbitrap Fusion Lumos (ThermoFisher) mass spectrometer, using the proxeon nanoflow source in positive ion mode. Peptides were introduced via a Pico-Tip Emitter 360 µm OD×20 µm ID; 10 µm tip (New Objective) and an applied spray voltage of 2.4 kV at capillary temperature at 275°C. Full mass scan was acquired with mass range 375–1500 *m*/z in profile mode with Orbitrap resolution of 60,000 and fill time at maximum of 50 ms. Data-dependent acquisition was performed with Orbitrap resolution at 15,000, fill time of 54 ms and a limitation of 10^5 ions. A normalized collision energy of 36 was applied and MS^2 data acquired in profile mode. For MS data analysis, IsobarQuant (Franken et al., 2015) and

Mascot (v2.2.07) were used to process the acquired data, which were searched against Uniprot *H. sapiens* UP000005640 proteome database, containing common contaminants and reversed sequences. Raw output files (protein.txt) of IsobarQuant were processed using the R programming language (ISBN 3-900051-07-0). Only proteins quantified with at least two unique peptides were used for data analysis. Raw signal-sums (signal_sum columns) were cleaned with the 'removeBatchEffect' function from the limma package (Ritchie et al., 2015) and further normalized using the variance stabilization normalization package (Huber et al., 2002). All experimental conditions were normalized separately to keep differences in protein abundance. Proteins were tested for differential expression using limma, based on false discovery rate (FDR) correction (Q=5%) and scoring a fold-change of at least 100% as a hit. The mass spectrometry proteomics data have been deposited to the ProteomeXchange Consortium via the PRIDE partner repository (EMBL-EBI) with the dataset identifier PXD019598.

Immunofluorescence and microscopy

For immunofluorescence, cells were grown on coverslips, fixed with 3.7% (w/v) paraformaldehyde in PHEM (30 mM HEPES, 65 mM PIPES, pH 6.9, 10 mM EGTA and 2 mM $MgCl_2$) for 10 min, permeabilized for 15 min with 0.5% v/v Triton X-100 in PHEM and immunolabeled with appropriate primary and secondary antibodies. Samples were analyzed with a Zeiss Apochromat 63×1.4 NA oil lens on a Zeiss Axiovert 200M inverted microscope with an AxioCam MRm camera.

Confocal imaging in Fig. 3D was carried out with a Zeiss LSM710 Axiovert confocal microscope using a 63× Plan-Neofluar 1.4 NA oil immersion objective lens, and in Fig. 4 with a Leica TCS SP2 DMIRE2 confocal microscope using 63×1.4 NA oil immersion objective lens.

Images were acquired with Zeiss Axiovision 4.2 software or LSM Zen or Leica LAS (v.4.1.0), processed using Adobe Photoshop CS6 and assembled into figures with Adobe Illustrator CS6.

Morphometric analysis and statistical evaluation

Fluorescence and morphology parameters [area, volume, oblate ellipticity, prolate ellipticity, sphericity and LBR (green)/Hoechst (blue) mean fluorescence intensity], as determined by Imaris (Bitplane AG, v 9.2.1), were compared in four independent experiments for a total of 103 cells (n=55 negative control treatment, n=48 *TMEM147* siRNA treatment) in stacks acquired on a Leica TCS SP2 DMIRE2 confocal microscope, using identical acquisition settings across samples. MANOVA using Pillai's test and α=0.05 (Addinsoft XLSTAT) was used to calculate the statistical difference between treatments (negative control and *TMEM147*-silencing), across all parameters. To assess statistical significance, individual parameters were analyzed by Mann–Whitney *U*-test (GraphPad Prism 8.0) with *P*-value adjustment using the FDR approach by the two-stage linear step-up procedure of Benjamini, Krieger and Yekutieli (Q=5%).

3D rendering of serial confocal *z*-stacks of HeLa nuclei (from the same control and *TMEM147*-silenced cells as above) was also performed with Imaris. 3D reconstruction of each nucleus was rendered using the 'new surface' algorithm with surface detail magnitude set at 0.250 µm and manual thresholding until voxels covered the entire surface of the nucleus according to LBR staining. Snapshots of 3D images were acquired to compare the localization of LBR in control and *TMEM147*-silenced cells. Elevated occurrence of ER localization for LBR labeling was tested by two-sided Fisher's exact test in Prism 8.0 (GraphPad) for the total of four independent experiments.

Lipidomics, cholesterol uptake analysis and statistical evaluation

For lipid analysis, 3×10^4–5×10^4 cells were used per condition. Acidic extractions were performed as previously described (Özbalci et al., 2013), in the presence of an internal lipid standard mix containing 50 pmol phosphatidylcholine (13:0/13:0, 14:0/14:0, 20:0/20:0; 21:0/21:0; Avanti Polar Lipids), 50 pmol sphingomyelin (d18:1 with N-acylated 13:0, 17:0, 25:0), 100 pmol D6-cholesterol (Cambridge Isotope Laboratory), 25 pmol phosphatidylinositol (16:0/16:0; Avanti Polar Lipids), 25 pmol phosphatidylethanolamine and 25 pmol phosphatidylserine (both 14:1/14:1, 20:1/20:1, 22:1/22:1), 25 pmol diacylglycerol (17:0/17:0; Larodan), 25 pmol cholesteryl ester (9:0, 19:0; Sigma), 24 pmol triacylglycerol (D5-Mix, LM-6000/D5-17:0/17:1/17:1; Avanti Polar Lipids), 5 pmol ceramide and 5 pmol glucosylceramide (both d18:1 with N-acylated 15:0, 17:0, 25:0), 5 pmol lactosylceramide (d18:1 with N-acylated C12 fatty acid), 10 pmol phosphatidic acid (21:0/22:6; Avanti Polar Lipids), 10 pmol phosphatidylglycerol (14:1/14:1, 20:1/20:1, 22:1/22:1) and 5 pmol lyso-phosphatidylcholine (17:1; Avanti Polar Lipids). Neutral extractions were performed in the presence of a phosphatidylethanolamine plasmalogen (PE P-)-containing standard mix, supplemented with 22 pmol PE P-Mix 1 (16:0p/15:0, 16:0p/19:0, 16:0p/25:0), 31 pmol PE P-Mix 2 (18:0p/15:0, 18:0p/19:0, 18:0p/25:0) and 43 pmol PE P-Mix 3 (18:1p/15:0, 18:1p/19:0, 18:1p/25:0). Lipid extracts were resuspended in 60 µl methanol, 2 µl-aliquots were diluted 1:10 in 96-well plates in methanol, and ammonium acetate was added to a final concentration of 10 mM. Samples were analyzed on a SCIEX QTRAP 6500+ mass spectrometer (Sciex, Canada) with chip-based (HD-D ESI Chip, Advion Biosciences, USA) nano-electrospray infusion and ionization via a Triversa Nanomate (Advion Biosciences, Ithaca, USA), employing precursor ion or neutral loss scanning as described (Özbalci et al., 2013). The remaining sample was evaporated and free cholesterol was subjected to acetylation and MS analysis as described previously (Özbalci et al., 2013). Data evaluation was undertaken using LipidView (ABSciex) and an in-house-developed software (ShinyLipids). Statistical evaluation of comparisons was assessed by multiple *t*-test with multiple testing correction, based on an FDR of <0.05 (Fig. 7).

For lipidomics, multivariate statistics analyses were performed in MetaboAnalyst version 4.0. All variables were log transformed and scaled by performing mean-centering and division by the standard deviation of each sample. All variables were then subjected to an unsupervised principal component analysis (PCA), generating a scores plot showing the variance in the dataset. The loadings plot for the generated model was used to determine which variables drive the separation between classes. The most discriminant variables were visualized using univariate statistics (Fig. S6).

For univariate statistics, GraphPad Prism 8.0 software was used. All data were expressed as mean±s.e.m. In GraphPad, one- or two-way ANOVA was performed where appropriate. For one-way ANOVA, Dunnett's post hoc multiple-comparisons test was performed, while for two-way ANOVA, Šidák's post hoc multiple-comparisons test was used (Fig. S6).

Cellular uptake of fluorescently tagged cholestrol was measured in three independent experiments using the Cholesterol Uptake Assay Kit (ab236212; Abcam) in a 96-well format, following the manufacturer's specifications. Briefly, cells were silenced for 48 h, subsequently incubated for a further 24 h with fluorescently tagged NBD-cholesterol at 20 µg/ml in either complete or serum-free medium or in the presence of cholesterol transport inhibitor U-18666A at 1 µM (as a positive control of increased retained cholesterol). NBD-cholesterol is an established probe for examining lipoprotein-mediated cholesterol uptake *in vivo* and in cultured cells (Frolov et al., 2000; Huang et al., 2015). Fluorescence emission readings with an FITC/GFP filter set were normalized to protein concentrations, determined for the same wells with bicinchonic acid (BCA) assays, followed by subtraction of background fluorescence. To assess statistical significance in uptake assays, multiple *t*-tests with multiple testing correction were performed (GraphPad Prism 8.0), using one unpaired *t*-test per row without assuming a consistent s.d. and applying the two-stage linear step-up procedure of Benjamini, Krieger and Yekutieli (Q=5%) to determine discovery (Fig. 7).

Cell growth assays

For the experiments shown in Fig. 7F,G, cells were seeded in multiple 24-well plates (15×10^3/well), grown in parallel either with control or *TMEM147* silencing and sampled by trypsination and counting in triplicate at time points 24 h, 48 h and 72 h post silencing. For each silencing regime, cells were either grown in complete medium for 72 h, or in complete medium for 48 h and under serum starvation until 72 h, or in complete medium for 48 h and under serum starvation until 72 h with the addition of exogenous cholesterol (20 µg/ml) at 64 h (i.e. for the last 8 h before sampling). Three independent experiments were performed and statistical evaluation was assessed for parametric (medium) comparisons after

confirming normality with the Shapiro–Wilk test, with one-way ANOVA based on the two-stage linear step-up procedure of Benjamini, Krieger and Yekutieli (Q=5%) to determine discovery (GraphPad Prism 8.0).

Acknowledgements
We are indebted to Prof. Iain W. Mattaj, in whose lab at the EMBL (Heidelberg) this project was initiated, for his kind and sustained support. We are grateful to Dr Chrysoula Pitsouli (University of Cyprus) for granting us access to a Leica confocal microscope SP2 and to Dr Jan Ellenberg (EMBL, Heidelberg) for providing the HeLa-LBR238-GFP cell line. We are thankful to Drs Mandy Rettel and Frank Stein for their expert assistance at the EMBL Proteomic Facility and Ms Anastasia Raoukka (University of Cyprus) for background work on TMEM147.

Competing interests
The authors declare no competing or financial interests.

Author contributions
Conceptualization: A.C., B.B., N.S.; Methodology: A.C., B.B., N.S.; Formal analysis: A.C., E.C., C.W.L., B.B.; Investigation: A.C., G.M., A.M., C.L., A.V., R.G.; Resources: A.C., C.H., N.S.; Writing - original draft: N.S.; Writing - review & editing: A.C., G.M., A.V., R.G., C.W.L., C.H., B.B., N.S.; Visualization: N.S.; Supervision: A.C., N.S.; Project administration: N.S.; Funding acquisition: N.S.

Funding
This work was supported by the University of Cyprus internal research funds (N.S.).

Data availability
The mass spectrometry proteomics data have been deposited to the ProteomeXchange Consortium via the PRIDE partner repository (EMBL-EBI) with the dataset identifier PXD019598.

Supplementary information
Supplementary information available online at
https://jcs.biologists.org/lookup/doi/10.1242/jcs.245357.supplemental

Peer review history
The peer review history is available online at
https://jcs.biologists.org/lookup/doi/10.1242/jcs.245357.reviewer-comments.pdf

References
Asencio, C., Davidson, I. F., Santarella-Mellwig, R., Ly-Hartig, T. B. N., Mall, M., Wallenfang, M. R., Mattaj, I. W. and Gorjánácz, M. (2012). Coordination of kinase and phosphatase activities by Lem4 enables nuclear envelope reassembly during mitosis. *Cell* **150**, 122-135. doi:10.1016/j.cell.2012.04.043

Bartoli, D., Piobbico, D., Bellet, M. M., Bennati, A. M., Roberti, R., Della Fazia, M. A. and Servillo, G. (2016). Impaired cell proliferation in regenerating liver of 3 β-hydroxysterol Δ14-reductase (TM7SF2) knock-out mice. *Cell Cycle* **15**, 2164-2173. doi:10.1080/15384101.2016.1195939

Baumann, O. and Walz, B. (2001). Endoplasmic reticulum of animal cells and its organization into structural and functional domains. *Int. Rev. Cytol.* **205**, 149-214. doi:10.1016/S0074-7696(01)05004-5

Bennati, A. M., Schiavoni, G., Franken, S., Piobbico, D., Della Fazia, M. A., Caruso, D., De Fabiani, E., Benedetti, L., Cusella De Angelis, M. G., Gieselmann, V. et al. (2008). Disruption of the gene encoding 3β-hydroxysterol Δ14-reductase (Tm7sf2) in mice does not impair cholesterol biosynthesis. *FEBS J.* **275**, 5034-5047. doi:10.1111/j.1742-4658.2008.06637.x

Blassberg, R., Macrae, J. I., Briscoe, J. and Jacob, J. (2016). Reduced cholesterol levels impair Smoothened activation in Smith-Lemli-Opitz syndrome. *Hum. Mol. Genet.* **25**, 693-705. doi:10.1093/hmg/ddv507

Boni, A., Politi, A. Z., Strnad, P., Xiang, W., Hossain, M. J. and Ellenberg, J. (2015). Live imaging and modeling of inner nuclear membrane targeting reveals its molecular requirements in mammalian cells. *J. Cell Biol.* **209**, 705-720. doi:10.1083/jcb.201409133

Braverman, N., Lin, P., Moebius, F. F., Obie, C., Moser, A., Glossmann, H., Wilcox, W. R., Rimoin, D. L., Smith, M., Kratz, L. et al. (1999). Mutations in the gene encoding 3β-hydroxysteroid-Δ8,Δ7-isomerase cause X-linked dominant Conradi-Hünermann syndrome. *Nat. Genet.* **22**, 291-294. doi:10.1038/10357

Capell-Hattam, I. M., Sharpe, L. J., Qian, L., Hart-Smith, G., Prabhu, A. V. and Brown, A. J. (2020). The cholesterogenic enzymes DHCR14 and LBR are differentially regulated transcriptionally and post-translationally. *J. Biol. Chem* **295**, 2850-2865. doi:10.1074/jbc.RA119.011323

Cascianelli, G., Villani, M., Tosti, M., Marini, F., Bartoccini, E., Magni, M. V. and Albi, E. (2008). Lipid microdomains in cell nucleus. *Mol. Biol. Cell* **19**, 5289-5295. doi:10.1091/mbc.e08-05-0517

Chen, S., Novick, P. and Ferro-Novick, S. (2013). ER structure and function. *Curr. Opin. Cell Biol.* **25**, 428-433. doi:10.1016/j.ceb.2013.02.006

Christodoulou, A., Santarella-Mellwig, R., Santama, N. and Mattaj, I. W. (2016). Transmembrane protein TMEM170A is a newly discovered regulator of ER and nuclear envelope morphogenesis in human cells. *J. Cell Sci.* **129**, 1552-1565. doi:10.1242/jcs.175273

Clever, M., Funakoshi, T., Mimura, Y., Takagi, M. and Imamoto, N. (2012). The nucleoporin ELYS/Mel28 regulates nuclear envelope subdomain formation in HeLa cells. *Nucleus* **3**, 187-199. doi:10.4161/nucl.19595

Codini, M., Cataldi, S., Lazzarini, A., Tasegian, A., Ceccarini, M. R., Floridi, A., Lazzarini, R., Ambesi-Impiombato, F. S., Curcio, F., Beccari, T. et al. (2016). Why high cholesterol levels help hematological malignancies: role of nuclear lipid microdomains. *Lipids Health Dis.* **15**, 4. doi:10.1186/s12944-015-0175-2

de Medina, P., Paillasse, M. R., Segala, G., Poirot, M. and Silvente-Poirot, S. (2010). Identification and pharmacological characterization of cholesterol-5,6-epoxide hydrolase as a target for tamoxifen and AEBS ligands. *Proc. Natl. Acad. Sci. USA* **107**, 13520-13525. doi:10.1073/pnas.1002922107

Dettmer, U., Kuhn, P.-H., Abou-Ajram, C., Lichtenthaler, S. F., Krüger, M., Kremmer, E., Haass, C. and Haffner, C. (2010). Transmembrane protein 147 (TMEM147) is a novel component of the Nicalin-NOMO protein complex. *J. Biol. Chem.* **285**, 26174-26181. doi:10.1074/jbc.M110.132548

Ellenberg, J., Siggia, E. D., Moreira, J. E., Smith, C. L., Presley, J. F., Worman, H. J. and Lippincott-Schwartz, J. (1997). Nuclear membrane dynamics and reassembly in living cells: targeting of an inner nuclear membrane protein in interphase and mitosis. *J. Cell Biol.* **138**, 1193-1206. doi:10.1083/jcb.138.6.1193

Fitzky, B. U., Witsch-Baumgartner, M., Erdel, M., Lee, J. N., Paik, Y.-K., Glossmann, H., Utermann, G. and Moebius, F. F. (1998). Mutations in the Delta7-sterol reductase gene in patients with the Smith-Lemli-Opitz syndrome. *Proc. Natl. Acad. Sci. USA* **95**, 8181-8186. doi:10.1073/pnas.95.14.8181

Franken, H., Mathieson, T., Childs, D., Sweetman, G. M., Werner, T., Tögel, I., Doce, C., Gade, S., Bantscheff, M., Drewes, G. et al. (2015). Thermal proteome profiling for unbiased identification of direct and indirect drug targets using multiplexed quantitative mass spectrometry. *Nat. Protoc.* **10**, 1567-1593. doi:10.1038/nprot.2015.101

Frolov, A., Petrescu, A., Atshaves, B. P., So, P. T. C., Gratton, E., Serrero, G. and Schroeder, F. (2000). High density lipoprotein mediated cholesterol uptake and targeting to lipid droplets in intact L-cell fibroblasts. *J. Biol. Chem.* **275**, 12769-12780. doi:10.1074/jbc.275.17.12769

Fukuhara, T., Hosoya, T., Shimizu, S., Sumi, K., Oshiro, T., Yoshinaka, Y., Suzuki, M., Yamamoto, N., Herzenberg, L. A., Herzenberg, L. A. et al. (2006). Utilization of host SR protein kinases and RNA-splicing machinery during viral replication. *Proc. Natl. Acad. Sci. USA* **103**, 11329-11333. doi:10.1073/pnas.0604616103

Ganger, M. T., Dietz, G. D. and Ewing, S. J. (2017). A common base method for analysis of qPCR data and the application of simple blocking in qPCR experiments. *BMC Bioinf.* **18**, 534. doi:10.1186/s12859-017-1949-5

Giannios, I., Chatzantonaki, E. and Georgatos, S. (2017). Dynamics and structure-function relationships of the Lamin B Receptor (LBR). *PLoS ONE* **12**, e0169626. doi:10.1371/journal.pone.0169626

Goyal, U. and Blackstone, C. (2013). Untangling the web: mechanisms underlying ER network formation. *Biochim. Biophys. Acta* **1833**, 2492-2498. doi:10.1016/j.bbamcr.2013.04.009

Hoffmann, K., Dreger, C. K., Olins, A. L., Olins, D. E., Shultz, L. D., Lucke, B., Karl, H., Kaps, R., Müller, D., Vayá, A. et al. (2002). Mutations in the gene encoding the lamin B receptor produce an altered nuclear morphology in granulocytes (Pelger-Huët anomaly). *Nat. Genet.* **31**, 410-414. doi:10.1038/ng925

Hoffmann, K., Sperling, K., Olins, A. L. and Olins, D. E. (2007). The granulocyte nucleus and lamin B receptor: avoiding the ovoid. *Chromosoma* **116**, 227-235. doi:10.1007/s00412-007-0094-8

Hu, J., Prinz, W. A. and Rapoport, T. A. (2011). Weaving the web of ER tubules. *Cell* **147**, 1226-1231. doi:10.1016/j.cell.2011.11.022

Huang, H., McIntosh, A. L., Landrock, K. K., Landrock, D., Storey, S. M., Martin, G. G., Gupta, S., Atshaves, B. P., Kier, A. B. and Schroeder, F. (2015). Human FABP1 T94A variant enhances cholesterol uptake. *Biochim. Biophys. Acta Mol. Cell Biol. Lipids* **1851**, 946-955. doi:10.1016/j.bbalip.2015.02.015

Huber, W., von Heydebreck, A., Sültmann, H., Poustka, A. and Vingron, M. (2002). Variance stabilization applied to microarray data calibration and to the quantification of differential expression. *Bioinformatics* **18** Suppl. 1r, S96-S104. doi:10.1093/bioinformatics/18.suppl_1.S96

Hubler, Z., Allimuthu, D., Bederman, I., Elitt, M. S., Madhavan, M., Allan, K. C., Shick, H. E., Garrison, E., Karl, M. T., Factor, D. C. et al. (2018). Accumulation of 8,9-unsaturated sterols drives oligodendrocyte formation and remyelination. *Nature* **560**, 372-376. doi:10.1038/s41586-018-0360-3

Hughes, C. S., Moggridge, S., Müller, T., Sorensen, P. H., Morin, G. B. and Krijgsveld, J. (2019). Single-pot, solid-phase-enhanced sample preparation for proteomics experiments. *Nat. Protoc.* **14**, 68-85. doi:10.1038/s41596-018-0082-x

Kedjouar, B., de Médina, P., Oulad-Abdelghani, M., Payré, B., Silvente-Poirot, S., Favre, G., Faye, J.-C. and Poirot, M. (2004). Molecular characterization of the microsomal tamoxifen binding site. *J. Biol. Chem.* **279**, 34048-34061. doi:10.1074/jbc.M405230200

Koczok, K., Gurumurthy, C. B., Balogh, I., Korade, Z. and Mirnics, K. (2019). Subcellular localization of sterol biosynthesis enzymes. *J. Mol. Histol.* **50**, 63-73. doi:10.1007/s10735-018-9807-y

Li, X., Roberti, R. and Blobel, G. (2015). Structure of an integral membrane sterol reductase from Methylomicrobium alcaliphilum. *Nature* **517**, 104-107. doi:10.1038/nature13797

Lin, S., Sun, S. and Hu, J. (2012). Molecular basis for sculpting the endoplasmic reticulum membrane. *Int. J. Biochem. Cell Biol.* **44**, 1436-1443. doi:10.1016/j.biocel.2012.05.013

Liu, X. Y., Dangel, A. W., Kelley, R. I., Zhao, W., Denny, P., Botcherby, M., Cattanach, B., Peters, J., Hunsicker, P. R., Mallon, A.-M. et al. (1999). The gene mutated in bare patches and striated mice encodes a novel 3β-hydroxysteroid dehydrogenase. *Nat. Genet.* **22**, 182-187. doi:10.1038/9700

Lukášová, E., Kovařík, A., Bačíková, A., Falk, M. and Kozubek, S. (2017). Loss of lamin B receptor is necessary to induce cellular senescence. *Biochem. J.* **474**, 281-300. doi:10.1042/BCJ20160459

Luo, J., Yang, H. and Song, B.-L. (2020). Mechanisms and regulation of cholesterol homeostasis. *Nat. Rev. Mol. Cell Biol.* **21**, 225-245. doi:10.1038/s41580-019-0190-7

Lynes, E. M. and Simmen, T. (2011). Urban planning of the endoplasmic reticulum (ER): how diverse mechanisms segregate the many functions of the ER. *Biochim. Biophys. Acta* **1813**, 1893-1905. doi:10.1016/j.bbamcr.2011.06.011

Ma, Y., Cai, S., Lv, Q., Jiang, Q., Zhang, Q., Sodmergen, Zhai, Z. and Zhang, C. (2007). Lamin B receptor plays a role in stimulating nuclear envelope production and targeting membrane vesicles to chromatin during nuclear envelope assembly through direct interaction with importin beta. *J. Cell Sci.* **120**, 520-530. doi:10.1242/jcs.03355

Makatsori, D., Kourmouli, N., Polioudaki, H., Shultz, L. D., Mclean, K., Theodoropoulos, P. A., Singh, P. B. and Georgatos, S. D. (2004). The inner nuclear membrane protein lamin B receptor forms distinct microdomains and links epigenetically marked chromatin to the nuclear envelope. *J. Biol. Chem.* **279**, 25567-25573. doi:10.1074/jbc.M313606200

Mattout, A., Cabianca, D. S. and Gasser, S. M. (2015). Chromatin states and nuclear organization in development-a view from the nuclear lamina. *Genome Biol.* **16**, 174. doi:10.1186/s13059-015-0747-5

Mimura, Y., Takagi, M., Clever, M. and Imamoto, N. (2016). ELYS regulates the localization of LBR by modulating its phosphorylation state. *J. Cell Sci.* **129**, 4200-4212. doi:10.1242/jcs.190678

Nikolakaki, E., Simos, G., Georgatos, S. D. and Giannakouros, T. (1996). A nuclear envelope-associated kinase phosphorylates arginine-serine motifs and modulates interactions between the lamin B receptor and other nuclear proteins. *J. Biol. Chem.* **271**, 8365-8372. doi:10.1074/jbc.271.14.8365

Nikolakaki, E., Mylonis, I. and Giannakouros, T. (2017). Lamin B receptor: interplay between structure, function and localization. *Cells* **6**, 28. doi:10.3390/cells6030028

Olins, A. L., Zwerger, M., Herrmann, H., Zentgraf, H., Simon, A. J., Monestier, M. and Olins, D. E. (2008). The human granulocyte nucleus: Unusual nuclear envelope and heterochromatin composition. *Eur. J. Cell Biol.* **87**, 279-290. doi:10.1016/j.ejcb.2008.02.007

Olins, A. L., Rhodes, G., Welch, D. B. M., Zwerger, M. and Olins, D. E. (2010). Lamin B receptor: multi-tasking at the nuclear envelope. *Nucleus* **1**, 53-70. doi:10.4161/nucl.1.1.10515

Ota, M., Tanaka, Y., Nakagawa, I., Jiang, J. J., Arima, Y., Kamimura, D., Onodera, T., Iwasaki, N. and Murakami, M. (2019). Chondrocytes play a role in the development of rheumatoid arthritis via TMEM147-mediated NF-kappaB activation. *Arthritis Rheumatol.* **72**, 931-942. doi:10.1002/art.41182

Özbalci, C., Sachsenheimer, T. and Brügger, B. (2013). Quantitative analysis of cellular lipids by nano-electrospray ionization mass spectrometry. *Methods Mol. Biol.* **1033**, 3-20. doi:10.1007/978-1-62703-487-6_1

Pantelidou, M., Zographos, S. E., Lederer, C. W., Kyriakides, T., Pfaffl, M. W. and Santama, N. (2007). Differential expression of molecular motors in the motor cortex of sporadic ALS. *Neurobiol. Dis.* **26**, 577-589. doi:10.1016/j.nbd.2007.02.005

Pfaffl, M. W., Horgan, G. W. and Dempfle, L. (2002). Relative expression software tool (REST(C)) for group-wise comparison and statistical analysis of relative expression results in real-time PCR. *Nucleic Acids Res.* **30**, e36. doi:10.1093/nar/30.9.e36

Platt, F. M., Wassif, C., Colaco, A., Dardis, A., Lloyd-Evans, E., Bembi, B. and Porter, F. D. (2014). Disorders of cholesterol metabolism and their unanticipated convergent mechanisms of disease. *Annu. Rev. Genomics Hum. Genet.* **15**, 173-194. doi:10.1146/annurev-genom-091212-153412

Prakash, A., Sengupta, S., Aparna, K. and Kasbekar, D. P. (1999). The erg-3 (sterol Δ14,15-reductase) gene of Neurospora crassa: generation of null mutants by repeat-induced point mutation and complementation by proteins chimeric for human lamin B receptor sequences. *Microbiology* **145**, 1443-1451. doi:10.1099/13500872-145-6-1443

Pyrpasopoulou, A., Meier, J., Maison, C., Simos, G. and Georgatos, S. D. (1996). The lamin B receptor (LBR) provides essential chromatin docking sites at the nuclear envelope. *EMBO J.* **15**, 7108-7119. doi:10.1002/j.1460-2075.1996.tb01102.x

Ritchie, M. E., Phipson, B., Wu, D., Hu, Y., Law, C. W., Shi, W. and Smyth, G. K. (2015). limma powers differential expression analyses for RNA-sequencing and microarray studies. *Nucleic Acids Res.* **43**, e47. doi:10.1093/nar/gkv007

Rosemond, E., Rossi, M., Mcmillin, S. M., Scarselli, M., Donaldson, J. G. and Wess, J. (2011). Regulation of M(3) muscarinic receptor expression and function by transmembrane protein 147. *Mol. Pharmacol.* **79**, 251-261. doi:10.1124/mol.110.067363

Santama, N., Er, C. P., Ong, L. L. and Yu, H. (2004). Distribution and functions of kinectin isoforms. *J. Cell Sci.* **117**, 4537-4549. doi:10.1242/jcs.01326

Schuler, E., Lin, F. and Worman, H. J. (1994). Characterization of the human gene encoding LBR, an integral protein of the nuclear envelope inner membrane. *J. Biol. Chem.* **269**, 11312-11317.

Shibata, Y., Voeltz, G. K. and Rapoport, T. A. (2006). Rough sheets and smooth tubules. *Cell* **126**, 435-439. doi:10.1016/j.cell.2006.07.019

Shultz, L. D., Lyons, B. L., Burzenski, L. M., Gott, B., Samuels, R., Schweitzer, P. A., Dreger, C., Herrmann, H., Kalscheuer, V., Olins, A. L. et al. (2003). Mutations at the mouse ichthyosis locus are within the lamin B receptor gene: a single gene model for human Pelger-Huet anomaly. *Hum. Mol. Genet.* **12**, 61-69. doi:10.1093/hmg/ddg003

Silva, I. T. G., Fernandes, V., Souza, C., Treptow, W. and Santos, G. M. (2017). Biophysical studies of cholesterol effects on chromatin. *J. Lipid Res.* **58**, 934-940. doi:10.1194/jlr.M074997

Silve, S., Dupuy, P. H., Labit-Lebouteiller, C., Kaghad, M., Chalon, P., Rahier, A., Taton, M., Lupker, J., Shire, D. and Loison, G. (1996). Emopamil-binding protein, a mammalian protein that binds a series of structurally diverse neuroprotective agents, exhibits Δ8-Δ7 sterol isomerase activity in yeast. *J. Biol. Chem.* **271**, 22434-22440. doi:10.1074/jbc.271.37.22434

Silve, S., Dupuy, P.-H., Ferrara, P. and Loison, G. (1998). Human lamin B receptor exhibits sterol C14-reductase activity in Saccharomyces cerevisiae. *Biochim. Biophys. Acta* **1392**, 233-244. doi:10.1016/S0005-2760(98)00041-1

Tint, G. S., Irons, M., Elias, E. R., Batta, A. K., Frieden, R., Chen, T. S. and Salen, G. (1994). Defective cholesterol biosynthesis associated with the Smith-Lemli-Opitz syndrome. *N. Engl. J. Med.* **330**, 107-113. doi:10.1056/NEJM199401133300205

Tsai, P.-L., Zhao, C., Turner, E. and Schlieker, C. (2016). The Lamin B receptor is essential for cholesterol synthesis and perturbed by disease-causing mutations. *eLife* **5**, e16011. doi:10.7554/eLife.16011

Tseng, L.-C. and Chen, R.-H. (2011). Temporal control of nuclear envelope assembly by phosphorylation of lamin B receptor. *Mol. Biol. Cell* **22**, 3306-3317. doi:10.1091/mbc.e11-03-0199

Ungricht, R., Klann, M., Horvath, P. and Kutay, U. (2015). Diffusion and retention are major determinants of protein targeting to the inner nuclear membrane. *J. Cell Biol.* **209**, 687-703. doi:10.1083/jcb.201409127

Wassif, C. A., Maslen, C., Kachilele-Linjewile, S., Lin, D., Linck, L. M., Connor, W. E., Steiner, R. D. and Porter, F. D. (1998). Mutations in the human sterol Δ7-reductase gene at 11q12-13 cause Smith-Lemli-Opitz syndrome. *Am. J. Hum. Genet.* **63**, 55-62. doi:10.1086/301936

Wassif, C. A., Brownson, K. E., Sterner, A. L., Forlino, A., Zerfas, P. M., Wilson, W. K., Starost, M. F. and Porter, F. D. (2007). HEM dysplasia and ichthyosis are likely laminopathies and not due to 3β-hydroxysterol Δ14-reductase deficiency. *Hum. Mol. Genet.* **16**, 1176-1187. doi:10.1093/hmg/ddm065

Waterham, H. R., Wijburg, F. A., Hennekam, R. C. M., Vreken, P., Poll-The, B. T., Dorland, L., Duran, M., Jira, P. E., Smeitink, J. A., Wevers, R. A. et al. (1998). Smith-Lemli-Opitz syndrome is caused by mutations in the 7-dehydrocholesterol reductase gene. *Am. J. Hum. Genet.* **63**, 329-338. doi:10.1086/301982

Worman, H. J., Yuan, J., Blobel, G. and Georgatos, S. D. (1988). A lamin B receptor in the nuclear envelope. *Proc. Natl. Acad. Sci. USA* **85**, 8531-8534. doi:10.1073/pnas.85.22.8531

Worman, H. J., Evans, C. D. and Blobel, G. (1990). The lamin B receptor of the nuclear envelope inner membrane: a polytopic protein with eight potential transmembrane domains. *J. Cell Biol.* **111**, 1535-1542. doi:10.1083/jcb.111.4.1535

Zwerger, M., Herrmann, H., Gaines, P., Olins, A. L. and Olins, D. E. (2008). Granulocytic nuclear differentiation of lamin B receptor-deficient mouse EPRO cells. *Exp. Hematol.* **36**, 977-987. doi:10.1016/j.exphem.2008.03.003